EVOLUTIONARY BIOLOGY

# Evolution of a ZW sex determination system in sticklebacks

**Xiaoqi Cheng[1,2], Ming Zou[1], Yu Wang[1], Yingnan Wang[3], Xinxin Li[1], Hongkai Zhang[1], Chongnv Wang[1], Juha Merilä[4,5], Baocheng Guo[1,2]***

Copyright © 2026 The Authors, some rights reserved; exclusive licensee American Association for the Advancement of Science. No claim to original U.S. Government Works. Distributed under a Creative Commons Attribution NonCommercial License 4.0 (CC BY-NC).

**The stickleback system offers a powerful model for investigating the evolutionary dynamics of sex chromosome differentiation. Although a ZW sex determination mechanism has previously been reported in sticklebacks, its origin and evolutionary history remain poorly resolved. Here, integrated multiomics analyses were applied to elucidate the evolutionary trajectory of the ZW system in *Pungitius sinensis* and *Pungitius bussei*. Using two newly assembled genomes and family-based segregation data, the sex-determining region (SDR) was delineated with high resolution. Several canonical genes implicated in sex determination pathways were located within the identified SDR, although the primary sex-determining gene could not be definitively identified. Phylogenomic evidence indicated that the ZW system emerged in *Pungitius* sticklebacks at least 5.0 million years ago. The absence of strong selective pressure may account for the limited differentiation between Z and W chromosomes. These findings define the evolutionary framework of the ZW system in *Pungitius* and contribute to a broader understanding of the extensive sex chromosome diversity in teleosts.**

## INTRODUCTION

Deciphering the evolutionary dynamics of sex chromosomes is essential for understanding both the mechanisms underlying sexual differentiation, such as sex determination and sexual selection, and the broader processes of biological diversification, such as reproductive isolation and speciation (*1*). The prevailing theoretical framework posits a stepwise progression in sex chromosome evolution: the emergence of a novel sex-determining locus and the initiation of recombination suppression between proto-sex chromosomes, which subsequently expands. This suppression leads to the accumulation of deleterious mutations and loss of gene content on the Y or W chromosome, giving rise to heteromorphic sex chromosomes and the evolution of dosage compensation systems. In certain lineages, degeneration proceeds to the point of complete Y or W chromosome loss (*2*–*4*). While this canonical model provides a conceptual scaffold, it represents a highly idealized trajectory that fails to capture the extensive variation observed across taxa (*1*, *3*, *5*). Moreover, several proposed steps within this model remain unresolved or actively debated, with the molecular mechanisms underlying key transitions still poorly understood.

Empirical research has revealed two major departures from the canonical model of sex chromosome evolution. First, comparative genomic studies have documented widespread and recurrent sex chromosome turnovers across diverse lineages, including teleosts [e.g., cichlids (*6*, *7*), fugu (*8*), and catfish (*9*)], boas and pythons (*10*, *11*), and anurans (*12*, *13*). This evolutionary fluidity has been attributed to various adaptive forces, including sexually antagonistic selection, meiotic drive, and heterozygote advantage, alongside nonadaptive processes such as genetic drift in small or bottlenecked populations (*14*). Second, growing evidence challenges the presumed relationship between the age of sex chromosomes and their degree of divergence. Notable examples include sturgeons (~180 million years old) (*15*), scallops (~350 million years old) (*16*), ratites (>100 million years old) (*17*), and toads (~46 million years ago) (*18*), all of which retain homomorphic sex chromosomes despite their ancient origins. These cases contradict the canonical expectation of inevitable recombination suppression and degeneration over time and raise unresolved questions about the mechanisms governing sex chromosome stability. Central among these are the processes that initiate recombination suppression and the forces that drive its subsequent expansion during sex chromosome evolution. Competing hypotheses suggest roles for both selective pressures—particularly sexually antagonistic selection—and neutral mechanisms (*19*, *20*). Proposed mechanisms underlying expansion include evolutionary forces such as the accumulation of sexually antagonistic loci and the emergence of compensatory regulatory architecture (*19*, *21*). In addition, structural rearrangements and transposable elements (TEs) constitute direct molecular mechanisms contributing to recombination suppression. Collectively, these insights emphasize the value of homomorphic sex chromosomes as critical systems for disentangling the early origins and diversification of sex chromosomes (*22*). Such systems provide a critical empirical foundation to test hypotheses regarding the origin of new sex chromosomes and to distinguish between recently evolved turnovers and ancient sex-determining systems that have remained refractory to differentiation (*3*, *23*).

Sticklebacks (Gasterosteidae) represent an exceptional system for elucidating the molecular dynamics of sex chromosome evolution due to their labile sex determination systems and the presence of both heteromorphic and homomorphic sex chromosomes (*24*–*30*). Within the genus *Pungitius*, both the chromosomal architecture and the genetic basis of sex determination exhibit notable variation (*25*). For instance, *Pungitius pungitius* exhibits an XY sex determination system (*24*–*26*), whereas members of the *sinensis* clade—descended from a common ancestor with *P. pungitius* approximately 10 million years ago (Mya) (*31*–*33*)—operate under a ZW system

[1]State Key Laboratory of Animal Biodiversity Conservation and Integrated Pest Management, Institute of Zoology, Chinese Academy of Sciences, Beijing 100101, China. [2]University of Chinese Academy of Sciences, Beijing 100049, China. [3]National Animal Collection Resource Center, Institute of Zoology, Chinese Academy of Sciences, Beijing 100101, China. [4]Area of Ecology and Biodiversity, School of Biological Sciences, University of Hong Kong, Hong Kong SAR, China. [5]Ecological Genetics Research Unit, Organismal and Evolutionary Biology Research Programme, Faculty of Biological and Environmental Sciences, University of Helsinki, Helsinki FI-00014, Finland.
*Corresponding author. Email: guobaocheng@ioz.ac.cn

with female heterogamety (*25*). Although the sex chromosomes in *Pungitius sinensis* and *Pungitius kaibarae* have been mapped genetically (*25*), their evolutionary origin and developmental trajectory remain largely unknown. In *P. sinensis*, minimal sequence divergence between Z and W chromosomes has been observed (*24*), raising key questions about whether this pattern reflects an early stage of sex chromosome differentiation or represents long-term stability without large-scale W degeneration. The robust phylogenetic framework available for sticklebacks (*31*–*33*) establishes *Pungitius* as an ideal lineage for investigating the genetic basis of sex chromosome emergence and divergence—or the unexpected lack thereof.

This study traced the evolutionary history of a ZW sex determination system in *Pungitius* with a multiomics approach. Chromosome-level genome assemblies for *P. sinensis* and its close relative *Pungitius bussei* were generated, enabling high-resolution delineation of the sex-determining region (SDR) in *P. sinensis* through integration with family-based segregation data. Within the SDR, gene content and repeat sequences were systematically annotated, and haplotype-resolved comparisons between Z and W chromosomes revealed both a female-specific region (FSR) and a highly divergent region (HDR). Comparative genomic analysis confirmed that the ZW system was shared by *P. sinensis* and *P. bussei*, indicating an origin of at least 5.0 Mya. Despite this evolutionary time span, the Z and W chromosomes remain largely undifferentiated, suggesting an absence of strong selective pressures favoring the expansion of recombination suppression. Collectively, these findings fill a critical gap in our understanding of sex chromosome evolution within the stickleback lineage and shed light on the evolutionary dynamics governing the unexpected stability of homomorphic sex chromosomes in teleosts.

## RESULTS

### Chromosome-level genome assemblies of *Pungitius* species

The genome size of *P. sinensis* was estimated at 496.7 Mb based on k-mer analysis, with *P. bussei* slightly smaller at 491.9 Mb. Genome-wide heterozygosity was 0.22% in *P. sinensis* and 0.19% in *P. bussei*. The final assembly of *P. sinensis* yielded 483 Mb across 218 contigs, with a contig N50 of 10.47 Mb and an estimated Benchmarking Universal Single-Copy Orthologs (BUSCO) completeness of 96.90% (*34*) (table S1). The *P. bussei* assembly totaled 502 Mb across 558 contigs, with a contig N50 of 5.67 Mb and an estimated BUSCO completeness of 97.40% (table S1). High-throughput chromosome conformation capture (Hi-C) data enabled anchoring of 462 Mb (95.60% of the 483 Mb *P. sinensis* assembly) and 494 Mb (98.45% of the 502 Mb *P. bussei* assembly) to 21 chromosomes, consistent with the haploid chromosome number previously reported for *P. pungitius* (*35*) (fig. S1). Repeat sequences accounted for 18.25% of the *P. sinensis* assembly and 15.41% of the *P. bussei* assembly. Kimura substitution profiles indicated that the proportion of repetitive sequences was higher in *Pungitius* than in *Gasterosteus aculeatus* (fig. S2). Gene annotation identified 23,244 protein-coding genes in *P. sinensis* and 24,456 in *P. bussei*, with gene, coding sequence, exon, and intron length distributions closely resembling those reported in previously assembled stickleback genomes (fig. S3). Together, these assemblies demonstrate sufficient quality for high-resolution comparative genomic analyses (table S1).

To place *Pungitius* genomic evolution within a phylogenetic framework, divergence times were inferred for six stickleback species with high-quality chromosome-level assemblies using 8395 single-copy orthologous protein-coding genes (Fig. 1A). The resulting phylogeny was consistent with earlier reconstructions (*31*, *32*, *36*). The most recent common ancestor (MRCA) of Gasterosteidae was estimated at 27.2 Mya, with a 95% highest posterior density (HPD) interval of 20.7 to 35.8 Mya. The MRCA of *Pungitius* was inferred to date to 8.6 Mya (HPD: 6.8 to 11.2 Mya), and divergence between *P. sinensis* and *P. bussei* was estimated at 5.0 Mya (HPD: 0.6 to 9.3 Mya).

### Extensive chromosomal rearrangements among stickleback genomes

To elucidate the contribution of large-scale chromosomal rearrangements to sex chromosome evolution in sticklebacks (*25*, *28*), a comprehensive, genome-wide synteny analysis was conducted across six species with high-quality, chromosome-level assemblies (Fig. 1A and table S1). Although broad macrosyntenic conservation was evident across the lineage, multiple lineage-specific rearrangements were detected (Fig. 1B), as observed previously (*36*). Chromosome 7 in *G. aculeatus* and chromosome 12 in *Pungitius* species each originated through independent chromosomal fusions. Chromosome 4, a region known to harbor loci involved in marine-freshwater ecological adaptation (*36*), arose via independent fusion events in both *G. aculeatus* and *Pungitius* lineages, indicating convergent chromosomal remodeling involving this region. Inversions were particularly prevalent between *P. pungitius* and *P. sinensis* (Fig. 1, A and B). Using non-*Pungitius* genomes as references, 39 and 54 inversions ≥5 kb were identified in the *P. sinensis* and *P. pungitius* genomes, respectively, found on 16 chromosomes in each case (Fig. 1B and table S2). Notably, several of these inversions were located within the SDRs on chromosome 12 in both species (Fig. 1C), which is known to facilitate the initiation of recombination suppression in the XY system of *P. pungitius* (*25*).

### SDR and female heterogametic sex determination system in *P. sinensis*

A female heterogametic (ZW) sex determination system was identified in *P. sinensis*, contrasting with the male heterogametic (XY) sex chromosome system observed in other stickleback species (*25*, *27*, *28*). Although chromosome 12 has been established as the sex chromosome in *P. sinensis*, the precise location of the SDR has remained unresolved, largely due to the limited sequence divergence between Z and W chromosomes in wild populations (*24*). To map the SDR, a family-cross panel comprising 16 males and 16 females from the Yoneshiro River population in Odate, Japan, was genotyped via whole-genome resequencing (WGR), yielding 1,262,057 high-quality single-nucleotide polymorphisms (SNPs) for downstream analyses.

The $F_{ST}$ between the sexes was highest within a 5-Mb segment on chromosome 12 (Chr12:2,000,000 to 7,000,000; Fig. 2, A and B), confirming this region as the putative SDR. Within this interval, sequencing depth analysis revealed pronounced differences in read coverage between females and males when aligned to the consensus sequence of chromosome 12 (Fig. 2C), suggesting sequence divergence between the Z and W chromosomes. In addition, principal components analysis (PCA) based on SNPs in 10-kb sliding windows across the SDR delineated individuals according to phenotypic sex, with the strongest differentiation observed within Chr12:2,400,000 to 4,800,000 (Fig. 2D). Although this SDR resided on chromosome 12 in both *P. sinensis* and *P. pungitius*, it occupied entirely distinct regions (Fig. 1C), demonstrating that SDR turnover has occurred within the genus.

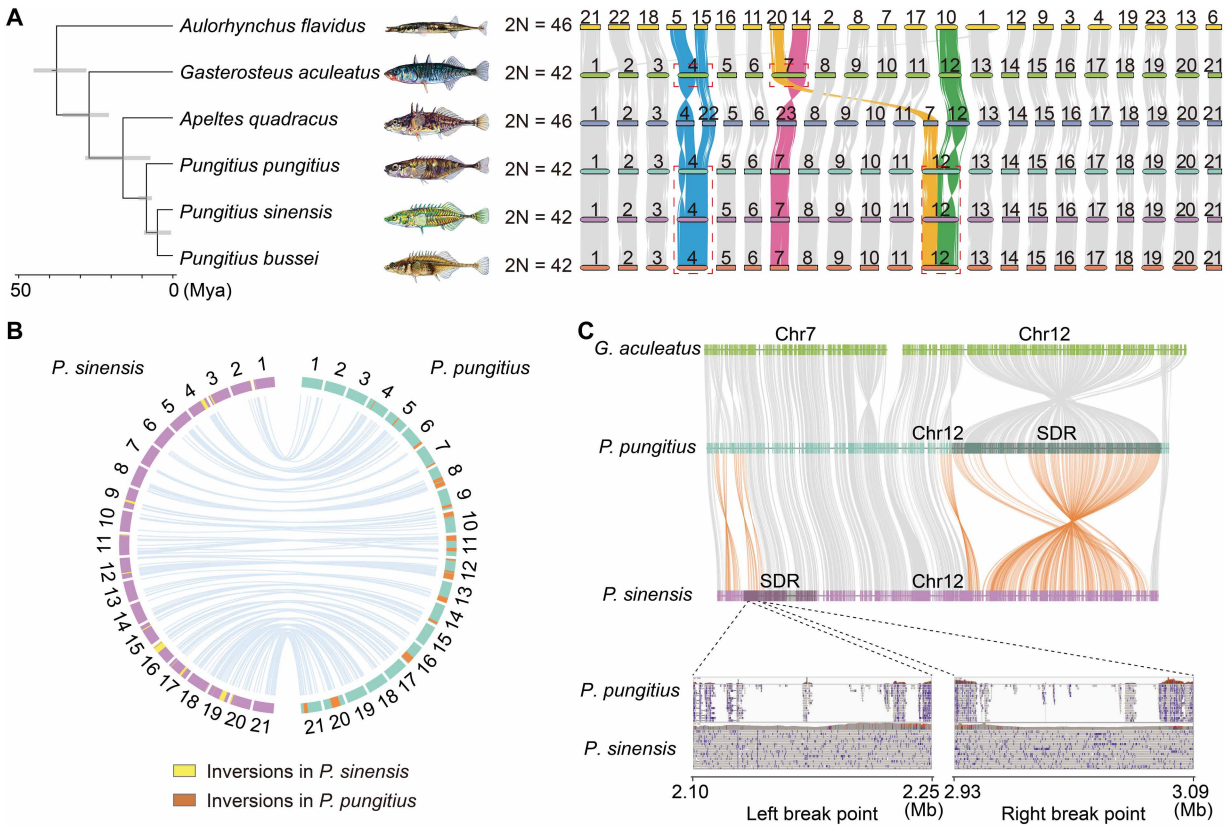


**Fig. 1. Synteny and chromosomal rearrangements among sticklebacks.** (**A**) Phylogeny and synteny of sticklebacks. The left panel shows maximum-likelihood phylogeny of stickleback species and their divergence times based on 8395 single-copy orthologous genes. The right panel shows macrosynteny across stickleback species, with karyotypes and chromosome names shown above. Chromosomal fusions are highlighted. The illustration of sticklebacks is reproduced with full permission from the original author (L. J. Hyun; https://galelee.carrd.co/#specimen). (**B**) Circos plot illustrating inverted genomic regions between *P. sinensis* and *P. pungitius*. Inversions in *P. sinensis* and *P. pungitius* are highlighted in yellow and brown, respectively. (**C**) Microsynteny of the chromosome 12 among *G. aculeatus*, *P. sinensis*, and *P. pungitius*. Sex-determining regions (SDRs) on chromosome 12 in *P. sinensis* and *P. pungitius* are shown. The bottom panel shows PacBio long-read mapping patterns consistent with breakpoints of an inversion that occurred in *P. pungitius*.

To determine the heterogametic pattern associated with the SDR, two independent analytical approaches were adopted. First, elevated heterozygosity in females was observed across this region, especially within Chr12:2,400,000 to 4,800,000 (Fig. 2E). Second, phylogenetic trees constructed from phased SNPs in 10-kb windows showed that, in the Chr12:2,400,000 to 4,800,000 region, half of the female-derived haplotypes formed a distinct clade, while the other half clustered with male haplotypes (Fig. 2F). Collectively, these findings provide strong support for a female heterogametic (ZW) sex determination system in *P. sinensis*. Notably, the signal of sex-specific differentiation was most pronounced within a core interval spanning approximately Chr12:2,400,000 to 4,800,000, indicating that the functional SDR is likely narrower than the initially defined boundary (Chr12:2,000,000 to 7,000,000). Nevertheless, the broader interval was retained in this study to capture the full range of genomic features potentially involved in sex determination, while recognizing that the principal functional SDR is likely confined to a more restricted segment.

## Divergence of the SDR between Z and W chromosomes in *P. sinensis*

To resolve the genomic architecture of the SDR in *P. sinensis*, haplotypes of chromosome 12 were assembled from the genome-sequenced female individual (table S3). On the basis of Illumina read depth patterns across the SDR in the family cross dataset, the longer haplotype was identified as the W chromosome (Fig. 3). Although the overall SDR sequence was largely conserved between the Z and W chromosomes, two distinct subregions, designated FSR and HDR, were resolved based on WGR read mapping differences between males and females (Fig. 3, B and C). Both regions exhibited sex-biased read depth; however, FSR was characterized by a pronounced difference in mapping coverage between the sexes and the presence of several haplotype-specific genes (Fig. 3, B and E). Repetitive element accumulation, including TEs and simple sequence repeats, is frequently implicated in sex chromosome divergence across both XY and ZW systems (*2*). Consistent with this trend, repeat content was notably enriched within the SDR (Fig. 3, A and D), with particularly elevated accumulation in the W-linked SDR compared to its Z-linked homolog (Wilcoxon test, $P = 0.00037$; Fig. 3, A and C). Despite broad conservation of gene synteny between the Z and W SDRs, haplotype-specific genes were identified within the FSR (fig. S4 and Fig. 3E). Specifically, two unique genes were present on the Z chromosome, while 11 were detected on the W chromosome, 7 of which were confined to the FSR (table S4). Of the seven FSR-restricted genes, six encode proteins containing the immunoglobulin V-set domains. In addition, the FSR showed marked enrichment

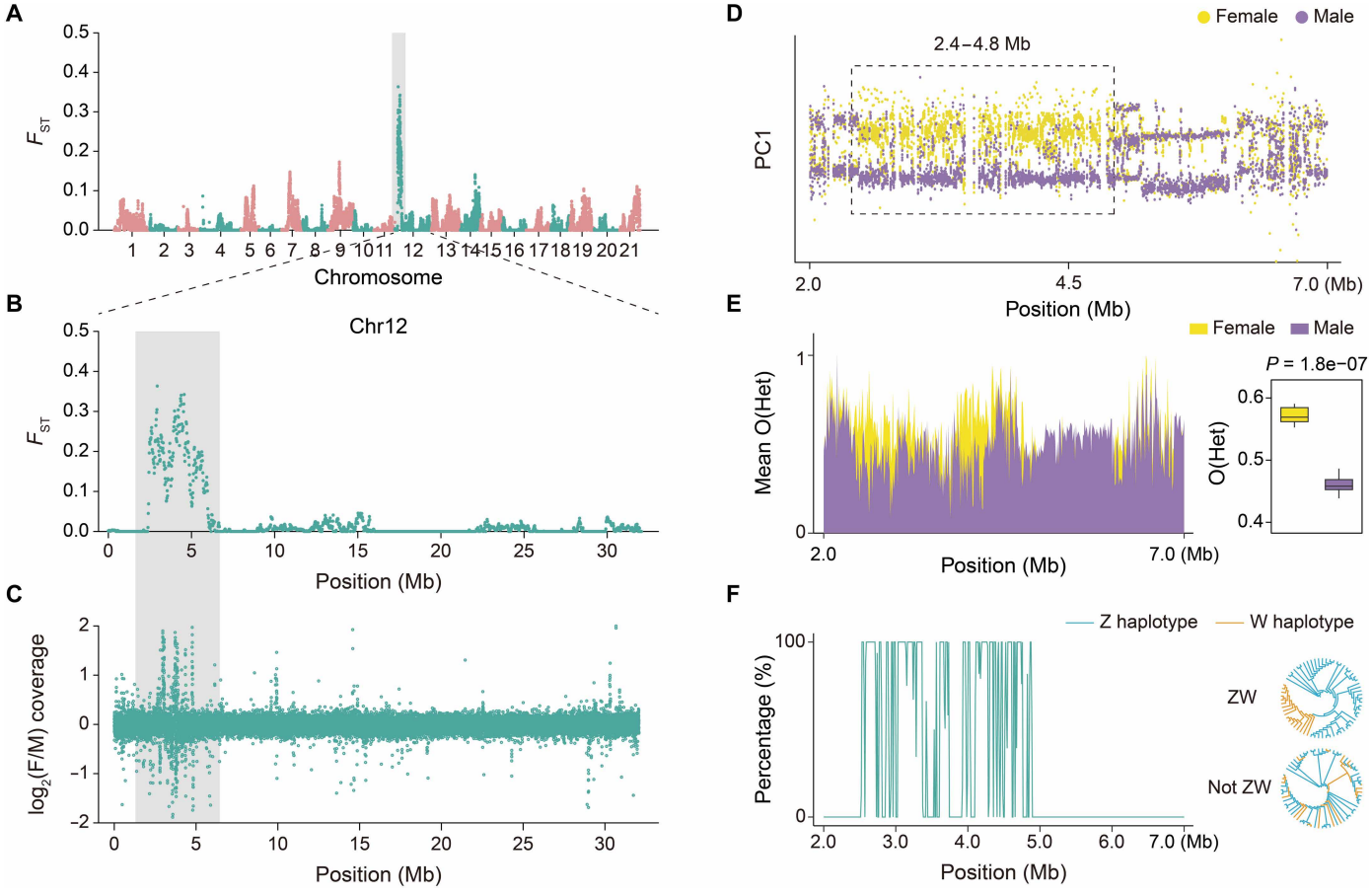


**Fig. 2. Identification of SDR in *P. sinensis* using genetic cross data.** (**A**) Genome-wide $F_{ST}$ values between females and males, with SDR on chromosome 12 highlighted. (**B**) $F_{ST}$ values between females and males along chromosome 12. (**C**) Differences in Illumina read coverage between sexes on chromosome 12. (**D**) PC1 values from a sliding-window PCA within the SDR. The highly divergent region between females and males (2.4 to 4.8 Mb) is indicated by a dashed box. (**E**) Left: Sliding-window analysis of average heterozygosity within the SDR, calculated per 10-kb window for females (yellow) and males (purple). Right: Boxplot comparing average individual heterozygosity between sexes within the core 2.4 to 4.8 Mb interval (Wilcox test, $P = 1.8 \times 10^{-7}$). (**F**) Percentage of ZW-consistent SNPs within the SDR. Examples of SNP trees consistent or inconsistent with ZW inheritance are shown.

of long terminal repeats (LTRs) (Fig. 3E and table S4). No haplotype-specific genes were detected within the HDR, although the region contained many repetitive sequences (fig. S5). These results collectively demonstrate that ZW divergence in *P. sinensis* remains limited.

## Genes associated with sex differentiation in the SDR in *P. sinensis*

A total of 352 protein-coding genes were annotated within the SDR, among which 159 exhibited sex-specific heterozygous sites and 168 showed sex-biased expression patterns (Fig. 4A and table S5). On the basis of comparative analysis, 18 genes were found exclusively in *P. sinensis*, lacking identifiable paralogs in syntenic regions of other stickleback genomes, with most encoding proteins of unknown function (table S5). Prior studies have documented sexually dimorphic traits in *P. sinensis*, including variation in body size (*37*) and nesting behavior (*38*). Notably, genes previously associated with these phenotypes (*39*, *40*) were not located within the SDR (table S5). Instead, 38 of the 352 genes mapped to the SDR have been implicated in sex differentiation and/or gonadal development according to earlier studies (table S6).

To investigate the potential involvement of these 38 genes in the evolution of the sex determination system in *P. sinensis*, their expression profiles in male and female gonads, levels of heterozygosity within the SDR, and WGR read depth patterns were analyzed (Fig. 4B and table S6). Additional signatures of selection were assessed through McDonald-Kreitman (MK) tests and nonsynonymous/synonymous ($d_N/d_S$) substitution rate analyses across stickleback species for lineage-specific adaptive changes. Among these candidates, 14 genes displayed expression patterns or functional attributes associated with sex differentiation or gonadal development (Fig. 4B). These comprised established regulators of sex determination or differentiation, including *dmrt4* (*41*, *42*), *cyp26b1* (*43*), and *nedd8* (*44*); genes exhibiting sex-biased expression, such as *ttc29* (*45*), *tesk1* (*46*), *mmp14* (*47*), *zp3* (*48*), *zpax4* (*49*), and *ybx2* (*50*); and genes implicated in gonadal development, including *acap1* (*51*), *ptgr1* (*52*), *svep1* (*46*), *capn5* (*53*), and *cbln1* (*54*). Three of these genes (*cyp26b1*, *tesk1*, and *svep1*) harbored sex-specific heterozygous variants within coding regions. An additional gene located within the SDR was also examined. Furthermore, gene *K02A2.6*, previously characterized as male-specific in cichlids (*7*) and located on the Y chromosome in *G. aculeatus*, was identified

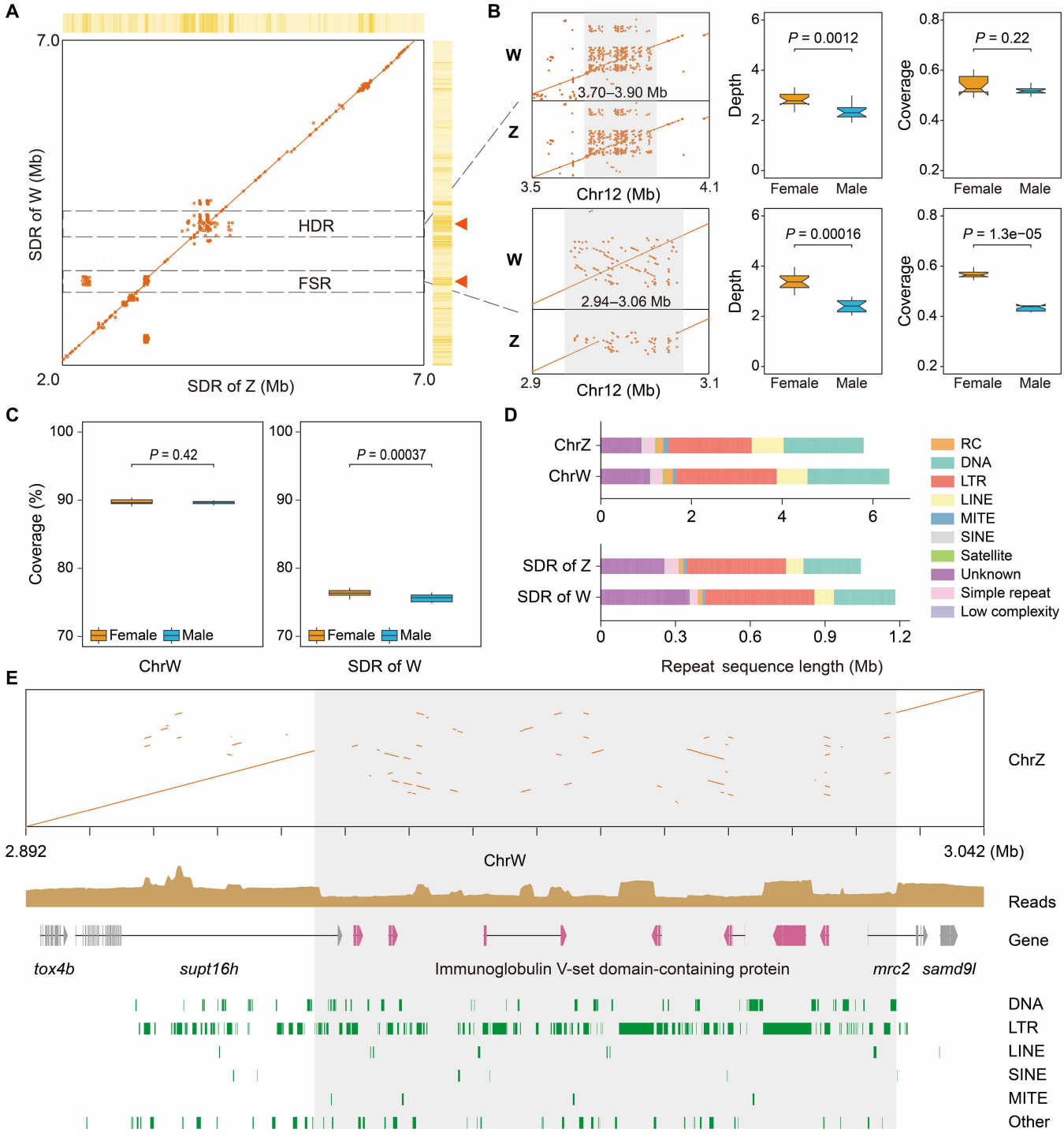


**Fig. 3. Haplotype-level differentiation of the SDR between Z and W chromosomes.** (**A**) Synteny between Z and W chromosome haplotypes within the SDR. Density of repeat sequences is indicated by bars. Female-specific region (FSR) and highly divergent region (HDR) on the W chromosome are marked with red triangles. (**B**) Synteny between ZW and consensus sequence in HDR and FSR. Illumina read depth and coverage differences between females and males in these regions are shown in the right panel. (**C**) Coverage differences between females and males across the W chromosome and SDR. Data are presented as boxplots from resequencing data aligned to the W haplotype genome. (**D**) Repeat composition of sex chromosomes, showing total length and repeat content of the Z and W chromosomes and their SDRs. (**E**) Genomic features of FSR, including (from top to bottom) microsynteny between Z and W haplotypes, PacBio read mapping depth, gene models, and repetitive elements.

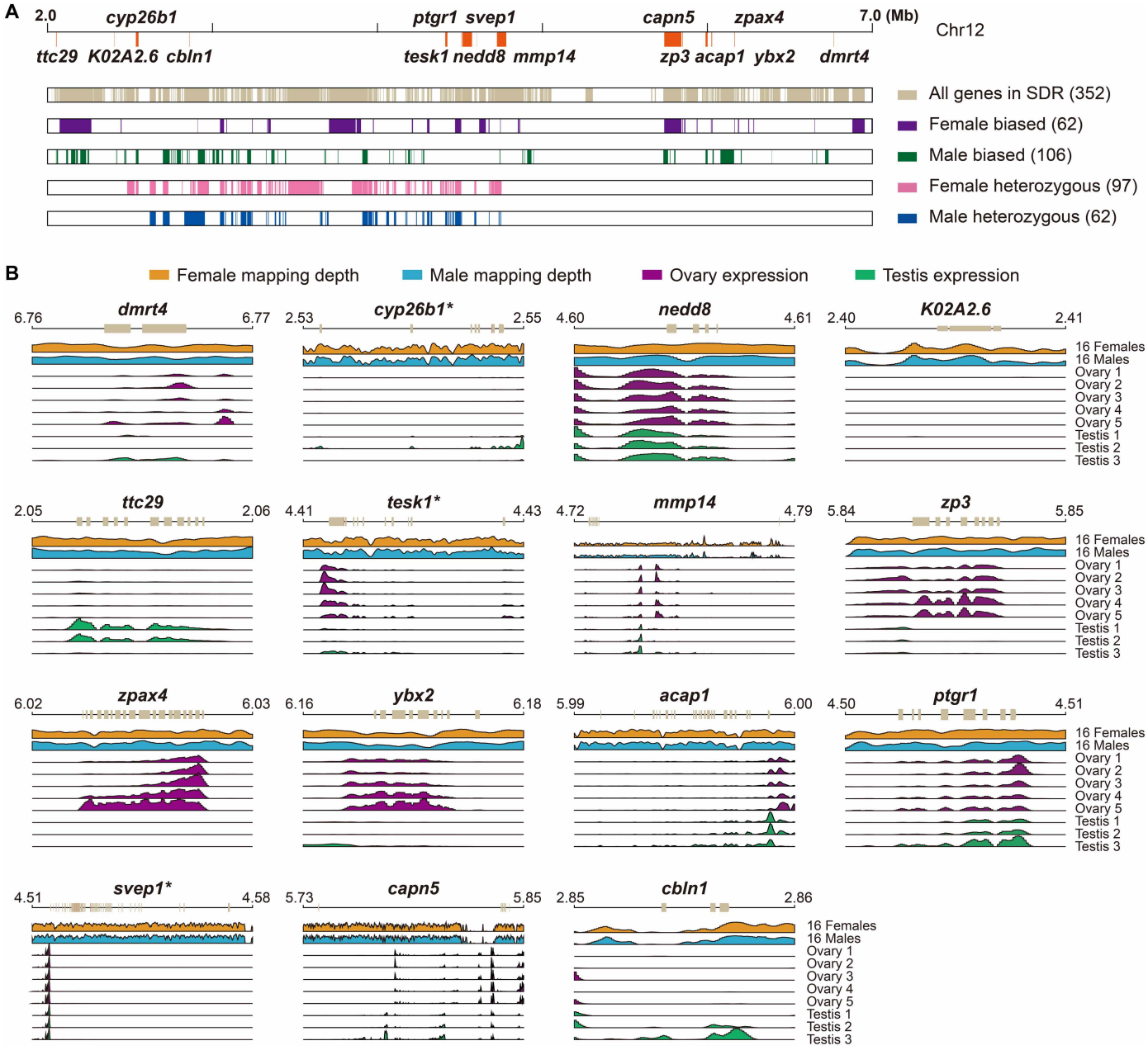


**Fig. 4. Candidate sex-determining genes within the SDR.** (**A**) Overview of annotated genes within the SDR. The top panel indicates positions of gene implicated in sex differentiation. Subsequent panels show all annotated genes in SDR, those with female-biased or male-biased expression, and genes containing female-specific or male-specific heterozygous sites. (**B**) Gene-specific characterization of sex-associated candidates. For each gene, the exon-intron structure is depicted at the top, followed by read mapping depth of WGR data from females and males, and read mapping depth of RNA-seq from gonadal tissues. Asterisks denote genes with sex-specific heterozygous variants located in exons.

within the *P. sinensis* SDR, although no expression was detected in gonadal tissue.

Among these candidates, *dmrt4* warranted particular consideration. Several members of the *dmrt* (Doublesex and Mab-3 related transcription factor) gene family, including *dmrt1* (*55*) and *dmrt4* (*41*, *42*), are widely recognized for conserved roles in sex determination and differentiation across teleosts. Although no sex-biased differences in expression, heterozygosity, or WGR read depth were observed between males and females in *P. sinensis*, species-specific amino acid substitutions were detected in *dmrt4* (fig. S6).

## Origin and evolution of the ZW sex chromosomes in *Pungitius* sticklebacks

The ZW sex determination system identified in *P. sinensis* has also been reported in other *Pungitius* sticklebacks within the *sinensis* clade distributed across northeast Asia, including *P. kaibarae* (*25*). To investigate whether this system originated in a shared ancestor or arose independently across lineages, chromosome 12 haplotypes were assembled from a female *P. bussei*, a species closely related to *P. sinensis* (*32*, *33*). Divergence between the two *P. bussei* haplotypes within the 2- to 7-Mb region of chromosome 12 (Fig. 5A) was

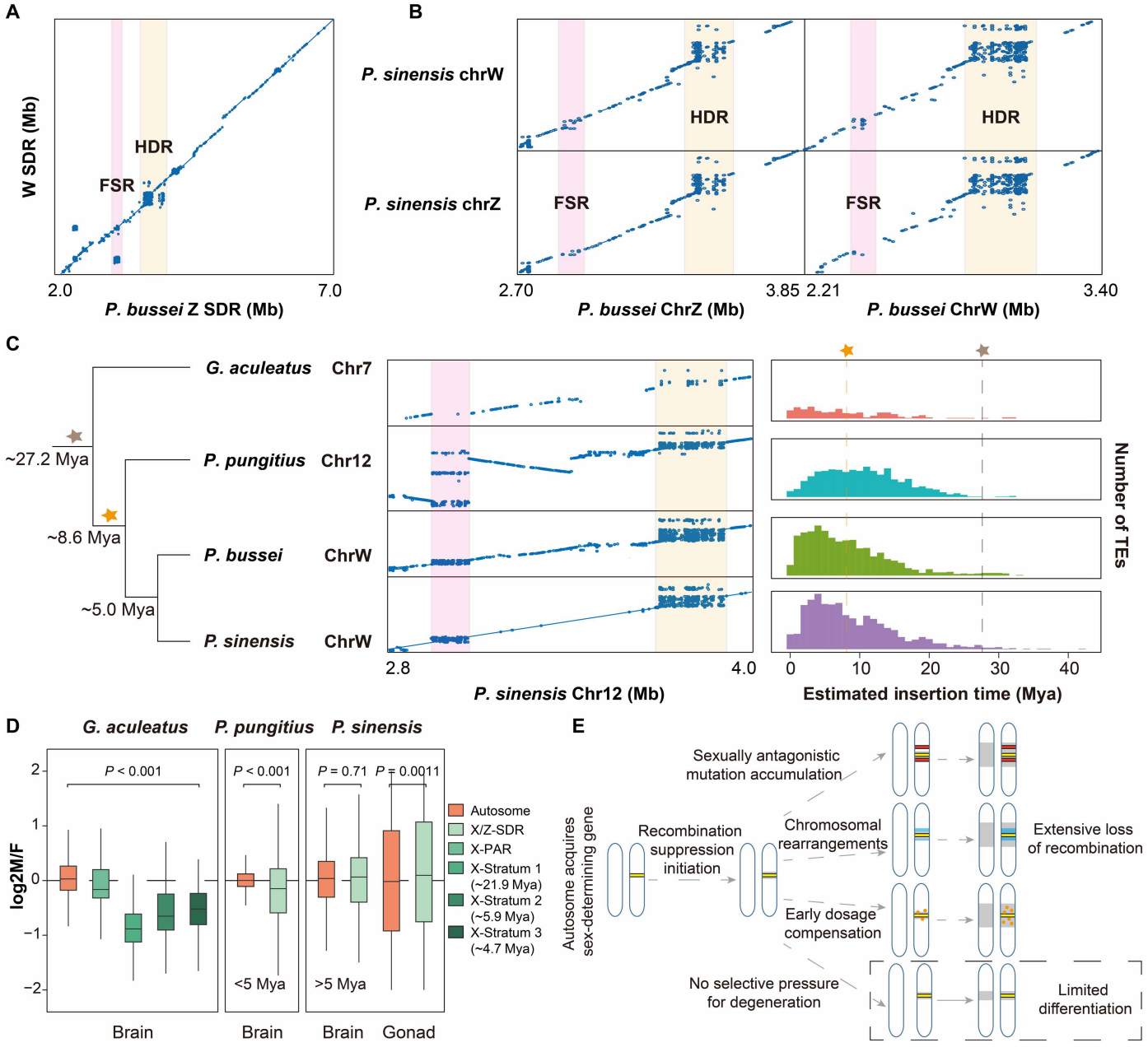


**Fig. 5. Shared origin and evolutionary dynamics of ZW sex chromosomes in *P. sinensis* and *P. bussei*.** (**A**) Haplotype synteny between Z and W chromosomes in the SDR in *P. bussei*, with the FSR and HDR highlighted in pink and orange, respectively. (**B**) SDR haplotype synteny between *P. sinensis* and *P. bussei*. (**C**) Repeat insertions within FSR and HDR across stickleback lineages. Left: Divergence times within sticklebacks, with MRCA of Gasterosteidae marked by a brown star and MRCA for *Pungitius* marked with an orange star. Center: Regional sequence alignments across stickleback species. Right: Estimated timing of W-specific repeat accumulation. (**D**) Expression profiles of autosomal and SDR genes in sticklebacks. Boxplots illustrate differences in gene expression between females and males within sex-determining (red) and autosomal regions (green) across sticklebacks. $\log_2$ (M/F): $\log_2$ (gene expression ratio between males and females). *P* value is from Bonferroni-corrected Wilcoxon rank-sum test. (**E**) Evolutionary trajectory of recombination suppression in sex chromosome of *P. sinensis* and *P. bussei*. Three mechanisms are proposed to facilitate expansion of the nonrecombining region: sexually antagonistic mutation accumulation, occurrence of chromosomal rearrangements, and early dosage compensation. In the absence of these factors, recombination suppression may still accumulate gradually through neutral processes.

consistent with the SDR structure observed in *P. sinensis* (Fig. 3A). Haplotype synteny comparisons further demonstrated that both species shared a homologous SDR (Fig. 5B). To reconstruct the evolutionary trajectory of this region, repeat landscapes within the FSR and HDR of *P. sinensis* and *P. bussei* were compared with homologous regions in other sticklebacks. Synteny analysis demonstrated a pronounced enrichment of repetitive elements within this region across all examined *Pungitius* species, whereas comparable repeats were largely absent in *G. aculeatus* (Fig. 5C). Insertion time estimates indicated that these repeat insertions occurred after the divergence of *Pungitius* from *G. aculeatus*, consistent with lineage-specific accumulation. Notably, a distinct burst of TE insertions was observed

at approximately 5 Mya in *P. sinensis* and *P. bussei*, coinciding with the inferred timing of sex chromosome emergence. This temporal correspondence suggests that repeat expansion accompanied progressive sex chromosome differentiation and recombination suppression. Together, these results indicate that the ZW system in *Pungitius* sticklebacks of the *sinensis* clade originated approximately 5.0 Mya in their common ancestor following divergence from *P. pungitius*.

In contrast to the frequent structural rearrangements between X and Y chromosomes in *P. pungitius* and *G. aculeatus* (*25*, *26*, *30*), no such inversions were detected between the Z and W chromosomes of the *sinensis* clade species. The high collinearity and conserved gene synteny between Z and W chromosomes at both interspecific and intraspecific levels (Figs. 3A and 5A) reinforce the conclusion that ZW differentiation remains minimal in this lineage. To evaluate the extent of sex chromosome differentiation at the molecular level, $d_N$ and $d_S$ substitution rates were compared across stickleback species. The sex chromosomes of *P. sinensis* were estimated to have formed approximately 5 Mya. However, despite this early origin, both $d_N$ and $d_S$ values in *P. sinensis* were apparently lower than those observed in the corresponding 5-Mya strata of *G. aculeatus* and *Gasterosteus wheatlandi*. Notably, divergence levels in *P. sinensis* were instead comparable to those reported in a considerably younger (~1 Mya) sex chromosome region in *G. wheatlandi* (table S7). This limited sequence divergence was also reflected at the transcriptional level (Fig. 5D). In both *G. aculeatus* and *P. pungitius*, genes located within the SDR displayed significantly female-biased expression relative to autosomal genes. In contrast, SDR-linked genes in *P. sinensis* exhibited no significant sex-biased expression, even though the SDR predates both stratum 3 of *G. aculeatus* [<4.7 Mya (*30*)] and the sex chromosome system of *P. pungitius* (<5.0 Mya) (*24*). Although the W chromosome in *P. sinensis* had accumulated TEs (Fig. 3C), it showed minimal evidence of degeneration and appeared to remain in an early, undifferentiated stage of sex chromosome evolution compared to the more advanced divergence observed in *G. aculeatus* and *P. pungitius* (Fig. 5D).

Expression profiles were then compared between brain and gonadal tissue in *P. sinensis*. PCA based on read counts indicated minimal expression divergence between sexes in the brain but marked differentiation in the gonads (fig. S7). In the gonads, 5288 genes were female biased and 5210 genes were male biased, encompassing genes involved in fundamental biological processes and sexual reproduction, such as sperm-zona pellucida binding (fig. S8). In contrast, only 561 female-biased genes and 274 male-biased genes were identified in the brain, including 10 female-biased and one male-biased gene located within the SDR. Given the relatively weak sexual dimorphism reported in *P. sinensis* (*56*, *57*), a corresponding reduction in sex-biased gene expression in nonreproductive tissues was hypothesized. To assess this, sex-biased expression of autosomal genes was compared between *P. sinensis* and *G. aculeatus*, a species characterized by pronounced phenotypic dimorphism. Unexpectedly, brain tissue of *P. sinensis* exhibited substantially higher numbers of sex-biased autosomal genes (551 female biased and 273 male biased) than *G. aculeatus* (43 female biased and 255 male biased), despite the markedly lower phenotypic dimorphism in *P. sinensis*. In contrast, gonadal tissues displayed largely comparable levels between species (*G. aculeatus*: 3885 female biased and 6027 male biased; *P. sinensis*: 5092 female biased and 5005 male biased). These findings indicate that the extent of sex-biased gene expression in brain tissue does not correspond directly to the degree of phenotypic sexual dimorphism across species, suggesting a more complex association than initially assumed.

Although the underlying mechanisms remain unresolved, these patterns are consistent with a distinct trajectory of sex chromosome evolution in *P. sinensis*. To place these observations in an evolutionary context, they were integrated into a conceptual framework (Fig. 5E) summarizing potential factors contributing to this process, as discussed below.

## DISCUSSION

The evolutionary trajectory of a ZW sex chromosome system in *Pungitius* sticklebacks was reconstructed through integrated genomic analyses. A female heterogametic configuration was identified in this lineage, in contrast to the male heterogametic (XY) system retained in most other stickleback species. Despite an estimated origin of at least 5.0 Mya, the Z and W chromosomes have remained largely homomorphic, exhibiting limited structural and sequence divergence. This pattern contrasts with the canonical model of sex chromosome evolution, which predicts progressive recombination suppression accompanied by W chromosome degeneration. These findings provide an empirical framework for reassessing current models of sex chromosome differentiation and refine understanding of the mechanisms underlying sex chromosome turnover and long-term evolutionary stability.

A female heterogametic system in *P. sinensis* was substantiated through genomic analyses, consistent with earlier molecular cytogenetic and linkage mapping evidence (*25*). In view of the predominance of male heterogamety across most other stickleback lineages, an ancestral XY configuration is implied for the family, with the ZW system arising subsequently within the *sinensis* clade of northeast Asian *Pungitius*. However, whether this transition occurred directly from an XY system or via other turnovers remains to be determined. To clarify the temporal origin of this transition, the evolutionary history of W-linked regions was examined using repeat-based dating approaches. Repetitive elements began accumulating in *Pungitius* approximately 20 Mya (Fig. 5C), generating repeat-rich genomic intervals that likely reduced local recombination (*58*). Following the divergence of *P. pungitius* from the common ancestor of *P. sinensis* and *P. bussei*, a pronounced expansion of repetitive elements occurred in the latter two lineages at approximately 5 Mya, coincident with the inferred onset of recombination suppression and early differentiation of sex chromosomes (Fig. 5C). Continued recombination restriction accompanied by repeat proliferation contributed to the formation of the FSR and the establishment of differentiated Z and W chromosomes (Figs. 3A and 5A). LTRs, which propagate through copy-and-paste mechanisms (*59*), represented the predominant class of TEs within the W-specific region (Fig. 3, D and E). This enrichment coincided with the presence of tandemly arranged W-specific genes and several encoding proteins containing immunoglobulin V-set domains (Fig. 3E and table S4). Proteins harboring V-set domains may share functional parallels with V-set and immunoglobulin domain containing protein 1 (*VSIG1*), located on the X chromosome in humans and mice and predominantly expressed in testicular germ cells (*60*). The biological roles of these W-linked genes in *P. sinensis*, and any potential relationship to LTR-associated genomic remodeling, remain unresolved and require further investigation to determine possible relevance to sex determination. It is important to note that delineation of the SDR was based on a limited

number of recombinant individuals derived from a single cross and may therefore overestimate its extent. Expanded analyses incorporating wild populations will be essential to refine SDR boundaries and to identify candidate sex-determining loci.

If the ZW system in *P. sinensis* indeed arose from an ancestral XY configuration, a scenario suggested by the phylogenetic context but requiring further validation, the forces precipitated such a shift remain unresolved. A newly arising sex-determining mutation can spread when it generates a sex ratio closer to the evolutionary optimum or enhances the viability of its carriers (*61*, *62*), thereby promoting sex determination transitions. Although these processes act directly on sex-determining loci, evaluating them in *P. sinensis* is challenging as the sex-determining genes have not yet been identified. An alternative pathway involves linkage between a sex-determining locus and sexually antagonistic variants, which can drive replacement of one sex determination system by another (*61*, *62*). This mechanism is improbable in *P. sinensis*, given the limited expression of sexually antagonistic dimorphisms in this species (*56*). Sex chromosome turnover may also occur when an established system acquires a substantial genetic load, prompting replacement, a process described under the hot-potato model (*63*). However, if a direct transition from XY to ZW did occur, this framework would be incompatible with the shift because it predicts retention of the ancestral heterogametic pattern (*63*). The transitions may instead have arisen through genetic drift (*61*, *62*), although empirical evidence will be required to evaluate this possibility.

In contrast to the linear degenerative pathway predicted by the canonical model, sticklebacks (Fig. 6) and many other teleosts exhibit frequent sex chromosome turnover, and most species retain sex chromosomes at an early stage of differentiation (*26*, *27*, *29*). The Z and W chromosomes of *P. sinensis* and *P. bussei* exhibited limited structural and sequence degeneration, particularly relative to sex-linked regions of comparable age in other stickleback lineages (table S7), consistent with persistence of a largely undifferentiated chromosomal state. Sexual antagonism is often considered as an important driver of sex chromosome evolution and has been documented across numerous vertebrate systems (*30*, *64*). The emergence of sexually antagonistic alleles near a sex-determining locus can generate advantageous allele combinations and promote the expansion of recombination suppression in sex chromosomes (*19*). In *P. sinensis*, several lines of evidence suggest limited sex-specific divergence, including weak phenotypic dimorphism (*56*), the absence of detectable accumulation of sexually antagonistic alleles within the sex-linked region (table S5), and comparatively modest expression differentiation between the sexes in brain tissue relative to gonadal tissue (Fig. 5D). Although these patterns do not constitute a direct quantification of sexually antagonistic selection, they are consistent with a scenario in which such selection operates at low intensity. This framework supports the interpretation that limited sexual antagonism may facilitate the persistence of homomorphic sex chromosomes; however, it is unlikely to represent the primary force underlying ZW differentiation in this lineage. Similar patterns have been reported in other teleosts, where recombination suppression between sex chromosomes has emerged in the apparent absence of strong sexually antagonistic selection (*65*).

However, the inference of weak sexually antagonistic selection in *P. sinensis* remains inconclusive. The presence of sex-specific dimorphism and sex-biased gene expression suggests that at least partial resolution of sexual conflict has occurred (*57*, *66*), yet unresolved conflicts may persist in regulatory or developmental dimensions not captured by differential expression between adult males and females. Furthermore, the transcriptomic analysis was limited in scope,

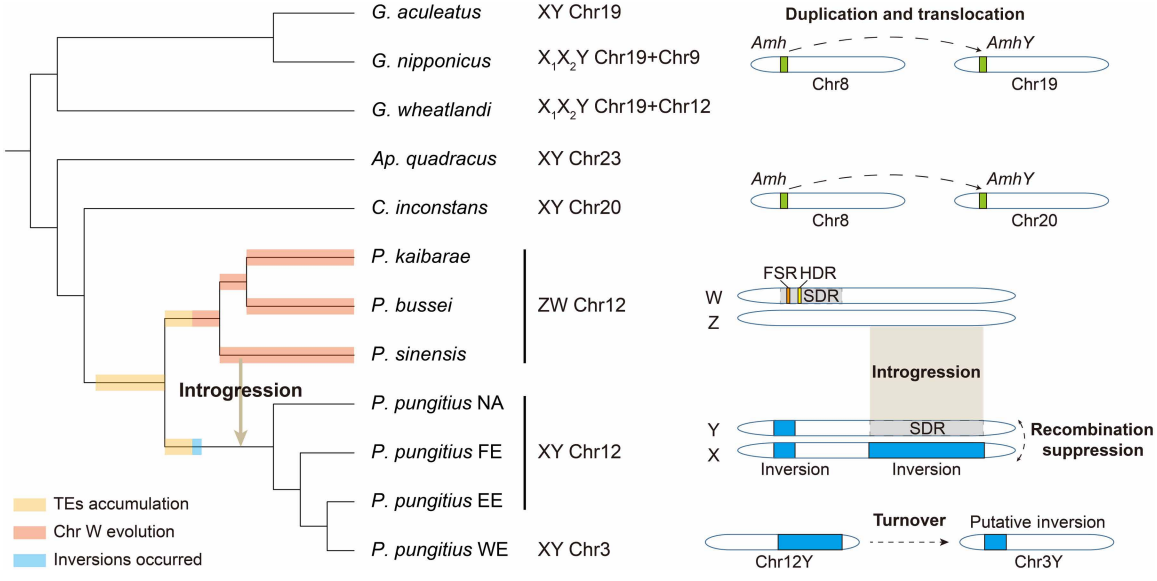


**Fig. 6. Sex chromosome evolution in sticklebacks.** The left panel illustrates the evolutionary history of sex chromosomes in the *sinensis* clade. Following an initial accumulation of transposable elements (TEs) in the ancestor of *Pungitius*, a ZW sex determination system emerged in the *sinensis* clade after divergence from the *pungitius* clade. Subsequently, the W chromosome evolved through further TE accumulation. Concurrently, several inversions emerged in *P. pungitius*. Following speciation, introgression from *P. sinensis* into *P. pungitius* facilitated sex-chromosome turnover in *P. pungitius*. The light orange shading indicates accumulation of TEs on chromosome 12 in the ancestor of *Pungitius* sticklebacks. The light red shading indicates the origin and evolution of W chromosome in *P. sinensis* and *P. bussei*, the light blue shading indicates inversions in *P. pungitius*, the brown arrow indicates introgression from *P. sinensis* to *P. pungitius*. The right panel shows diversity of sex chromosomes in *G. aculeatus*, *G. wheatlandi*, *G. nipponicus*, *A. quadracus*, *C. inconstans*, *P. kaibarae*, *P. bussei*, *P. sinensis*, and *P. pungitius*, summarized from this and earlier studies (*24*–*30*).

lacking representation across multiple tissues and developmental stages, which restricts the ability to assess the breadth of sex-specific regulatory divergence (*57*, *66*). Reliance on gene function annotation and trait-level associations to infer sexually antagonistic loci may also be insufficient, given the limited understanding of the genomic underpinnings of sexually antagonistic phenotypes in most systems (*67*). As such, the contribution of sexually antagonistic selection to ZW chromosome differentiation in *P. sinensis* cannot be excluded, and resolving its role will require broader developmental, genomic, and ecological datasets.

In addition, regions of suppressed recombination can originate and expand through genetic drift (*20*). For example, a randomly arising inversion that overlaps a sex-determining locus can, in principle, stabilize and expand nonrecombining segments, although such inversions are often viewed as secondary consequences rather than initial drivers of recombination suppression (*68*). No inversion was detected in *P. sinensis* (Figs. 3A and 5A), yet substantial accumulation of TEs was observed between the Z and W chromosomes (Fig. 5, A and B). TE deposition in this region began before species divergence within *Pungitius*, indicating the presence of a preexisting genomic interval characterized by reduced recombination (Fig. 5C). Such an interval could have created a permissive environment for the initiation of ZW differentiation (*20*). Demographic history may further support this scenario. Species within the *sinensis* clade are believed to have historically maintained small effective population sizes (*32*, *33*), conditions under which drift can facilitate rapid fixation of TE insertions, thereby increasing the likelihood that recombination suppression becomes established (*20*). However, TE accumulation ceased relatively early in both *P. sinensis* and *P. bussei* (Fig. 5C), indicating that the subsequent expansion of recombination suppression was arrested.

The persistence of homomorphic sex chromosomes in the *sinensis* clade of *Pungitius* sticklebacks might result from other mechanisms. For example, dosage compensation, which typically evolves to counterbalance gene dosage imbalances resulting from sex chromosome degeneration, can, in some cases, accelerate divergence if established during early stages of sex chromosome evolution (*21*). In contrast, failure to evolve dosage compensation may constrain divergence, as shown in ratites such as ostriches (*69*). In *P. sinensis*, the absence of significant differences between SDR-linked and autosomal genes in somatic tissues suggests that the W chromosome has not undergone substantial degeneration and that compensatory mechanisms are likely unnecessary. Recurrent recombination through sex reversal has been implicated in maintaining undifferentiated sex chromosomes in frogs (*70*), but sex-reversed individuals have not been documented in *Pungitius*, reducing the plausibility of this mechanism. Another possibility involves the accumulation of reversibly sex-biased genes during gonadal development within the SDR, a mechanism proposed to contribute to the persistence of homomorphic sex chromosomes in mollusks (*16*). A similar process may operate in *Pungitius*, as multiple genes within the SDR exhibit sex-biased expression in gonadal tissue. However, the temporal dynamics and reversibility of this expression remain uncharacterized. Comprehensive transcriptomic analyses spanning additional tissues and developmental stages will be required to rigorously assess the applicability of this model in *P. sinensis*.

Overall, this study delineated the evolutionary history of a derived ZW sex determination system in *Pungitius*, characterized by limited differentiation between Z and W chromosomes. These findings point to weak sexually antagonistic selection, absence of major structural rearrangements, and lack of early dosage compensation in the SDR as key factors constraining divergence. These results expand the current understanding of sex chromosome evolution by highlighting an alternative trajectory in which homomorphy can persist despite the presence of a long-established SDR, thus offering additional insights into the evolutionary dynamics of teleost sex chromosomes.

## MATERIALS AND METHODS

### Sampling and sequencing

A female *P. sinensis* specimen was collected from Xinlong, Henan Province, China (117°20′E, 40°24′N), and a female *P. bussei* specimen was collected from Yichun, Heilongjiang Province, China (128° 42′10″E, 47°44′21″N) for genome sequencing and assembly. To identify sex-linked regions, WGR was performed on 32 individuals (16 males and 16 females) from a single family of *P. sinensis* originating from the Yoneshiro River in Odate, Japan. Genomic DNA was extracted from muscle tissue using a DNeasy Blood & Tissue Kit (Qiagen). Long-read sequencing was conducted on the PacBio Sequel II platform and paired-end short-read sequencing was conducted on the Illumina NovaSeq 6000 platform. RNA from brain, liver, muscle, and gonad tissues was extracted and sequenced for gene annotation and expression quantification. Sample information and genomic datasets are summarized in table S8. All samples were obtained in accordance with national and institutional ethical regulations with permission from the Finnish Food Safety Authority (#2736/425/2007, #1181/0527/2011, and #3701/0460/2011). All animal experiments were conducted under license from the Finnish National Animal Experiment Board (#STH379A and #PH1236A).

### Genome assembly and annotation

After quality control and genome size estimation, assemblies were generated for *P. sinensis* and *P. bussei*. Genome annotation was conducted by integrating evidence from ab initio predictions, homology-based searches, and transcriptomic evidence. Repetitive elements were identified using EDTA (v1.9.7) (*71*) and RepeatMasker (v4.1.1).

### Comparative genomics

Single-copy orthologs were identified across stickleback genomes. Maximum-likelihood phylogenetic inference was performed using concatenated multisequence alignments of these genes, with the optimal substitution model selected automatically. Divergence times were estimated using fossil record calibrations and previous published research. Syntenic relationships among sticklebacks were assessed based on coding sequence alignments. Chromosomal inversions between *P. sinensis* and *P. pungitius* were identified, retaining only those ≥5 kb.

### Identification of the sex-linked region

WGR data from the 32 *P. sinensis* individuals were aligned to the *P. sinensis* reference genome to identify sex-linked regions (table S8). SNPs were called, and sex-specific differentiation was quantified by calculating the fixation index ($F_{ST}$) and coverage differences between the sexes along chromosome 12 in nonoverlapping 10-kb sliding

windows. PCA, heterozygosity estimation, and haplotype phylogeny reconstruction were also performed within this region using the same window strategy.

### Haplotype assembly and comparative analysis

To better understand sex chromosome evolution, haploid assemblies of chromosome 12 were generated for both *P. sinensis* and *P. bussei*. Pairwise alignment of haplotypes identified regions of sex-specific differentiation. Illumina reads from individuals of the crossed family were mapped to the W haplotype to evaluate coverage differences. Repetitive sequences and protein-coding genes in haploid assemblies were annotated using the same pipeline as for the full genome. Gene content was compared between haplotypes using reciprocal BLASTP.

### Characterization of sex-linked genes

RNA sequencing (RNA-seq) data from the gonadal and brain tissues were mapped to the corresponding assemblies. Transcriptome assemblies and differential expression analyses were performed for each tissue. Gene functions within the sex-linked region were retrieved via Google Scholar to assess potential involvement in sex determination. Average read depth and coverage for these genes were compared between sexes. Nonsynonymous and synonymous substitution rates of each gene in *P. sinensis* were compared to orthologs in other sticklebacks to assess selective pressures (*72*). The MK test was applied to detect potentially positive selection in females using cmktest (https://github.com/jhpanda/McDonaldKreitmanTest), in which the female population was treated as the target and the male population as the outgroup.

### Estimation of sex-specific TE insertion time

Repeat elements within differentiated regions of chromosome 12 in *P. sinensis* and *P. bussei* were similarly analyzed. Corresponding orthologous regions in *G. aculeatus* and *P. pungitius* were extracted. Divergence between female-specific repeats and consensus sequences was calculated using RepeatMasker. Insertion times were estimated according to Kimura's two-parameter model (*73*)

$$K = -\frac{1}{2}\ln\{(1-2P-Q)\sqrt{1-2Q}\} \quad (1)$$

$$T = K/(2r) \quad (2)$$

where $P$ is the transition rate, $Q$ is the transversion rate, $K$ is Kimura divergence, $T$ is the insertion time, and $r$ is the substitution rate, set to $7.1 \times 10^{-3}$ substitutions per synonymous site per million years (*74*).

## Supplementary Materials

**The PDF file includes:**

Supplementary Text
Figs. S1 to S8
Legends for tables S1 to S8
References

**Other Supplementary Material for this manuscript includes the following:**

Tables S1 to S8

## REFERENCES


1. J. Wang, W. Tao, T. D. Kocher, D. Wang, Sex chromosome turnover and biodiversity in fishes. *J. Genet. Genomics* **51**, 1351–1360 (2024).
2. D. Charlesworth, B. Charlesworth, G. Marais, Steps in the evolution of heteromorphic sex chromosomes. *Heredity* **95**, 118–128 (2005).
3. Z. Zhu, L. Younas, Q. Zhou, Evolution and regulation of animal sex chromosomes. *Nat. Rev. Genet.* **26**, 59–74 (2025).
4. J. K. Abbott, A. K. Nordén, B. Hansson, Sex chromosome evolution: Historical insights and future perspectives. *Proc. R. Soc. B* **284**, 20162806 (2017).
5. B. Vicoso, Molecular and evolutionary dynamics of animal sex-chromosome turnover. *Nat. Ecol. Evol.* **3**, 1632–1641 (2019).
6. A. El Taher, F. Ronco, M. Matschiner, W. Salzburger, A. Böhne, Dynamics of sex chromosome evolution in a rapid radiation of cichlid fishes. *Sci. Adv.* **7**, eabe8215 (2021).
7. A. Böhne, A. A.-T. Weber, J. Rajkov, M. Rechsteiner, A. Riss, B. Egger, W. Salzburger, Repeated evolution versus common ancestry: Sex chromosome evolution in the haplochromine cichlid *Pseudocrenilabrus philander*. *Genome Biol. Evol.* **11**, 439–458 (2019).
8. A. Kabir, R. Ieda, S. Hosoya, D. Fujikawa, K. Atsumi, S. Tajima, A. Nozawa, T. Koyama, S. Hirase, O. Nakamura, M. Kadota, O. Nishimura, S. Kuraku, Y. Nakamura, H. Kobayashi, A. Toyoda, S. Tasumi, K. Kikuchi, Repeated translocation of a supergene underlying rapid sex chromosome turnover in *Takifugu* pufferfish. *Proc. Natl. Acad. Sci. U.S.A.* **119**, e2121469119 (2022).
9. S. Zheng, H. Tao, Y. Song, M. Li, H. Yang, J. Li, H. Yan, B. Sheraliev, W. Tao, Z. Peng, Y. Zhang, D. Wang, The origin, evolution, and translocation of sex chromosomes in *Silurus* catfish mediated by transposons. *BMC Biol.* **23**, 54 (2025).
10. T. Gamble, T. A. Castoe, S. V. Nielsen, J. L. Banks, D. C. Card, D. R. Schield, G. W. Schuett, W. Booth, The discovery of XY sex chromosomes in a boa and python. *Curr. Biol.* **27**, 2148–2153.e4 (2017).
11. T. Pšenička, B. Augstenová, D. Frynta, P. Kornilios, L. Kratochvíl, M. Rovatsos, Sex chromosome turnovers and stability in snakes. *Mol. Biol. Evol.* **42**, msae273 (2025).
12. D. L. Jeffries, G. Lavanchy, R. Sermier, M. J. Sredl, I. Miura, A. Borzée, L. N. Barrow, D. Canestrelli, P.-A. Crochet, C. Dufresnes, J. Fu, W.-J. Ma, C. M. Garcia, K. Ghali, A. G. Nicieza, R. P. O'Donnell, N. Rodrigues, A. Romano, Í. Martínez-Solano, I. Stepanyan, S. Zumbach, A. Brelsford, N. Perrin, A rapid rate of sex-chromosome turnover and non-random transitions in true frogs. *Nat. Commun.* **9**, 4088 (2018).
13. W.-J. Ma, P. Veltsos, The diversity and evolution of sex chromosomes in frogs. *Genes* **12**, 483 (2021).
14. J. Kitano, S. Ansai, Y. Takehana, Y. Yamamoto, Diversity and convergence of sex-determination mechanisms in teleost fish. *Annu. Rev. Anim. Biosci.* **12**, 233–259 (2024).
15. H. Kuhl, Y. Guiguen, C. Höhne, E. Kreuz, K. Du, C. Klopp, C. Lopez-Roques, E. S. Yebra-Pimentel, M. Ciorpac, J. Gessner, D. Holostenco, W. Kleiner, K. Kohlmann, D. K. Lamatsch, D. Prokopov, A. Bestin, E. Bonpunt, B. Debeuf, P. Haffray, R. Morvezen, P. Patrice, R. Suciu, R. Dirks, S. Wuertz, W. Kloas, M. Schartl, M. Stöck, A 180 Myr-old female-specific genome region in sturgeon reveals the oldest known vertebrate sex determining system with undifferentiated sex chromosomes. *Philos. Trans. R. Soc. Lond. B Biol. Sci.* **376**, 20200089 (2021).
16. W. Han, L. Liu, J. Wang, H. Wei, Y. Li, L. Zhang, Z. Guo, Y. Li, T. Liu, Q. Zeng, Q. Xing, Y. Shu, T. Wang, Y. Yang, M. Zhang, R. Li, J. Yu, Z. Pu, J. Lv, S. Lian, J. Hu, X. Hu, Z. Bao, L. Bao, L. Zhang, S. Wang, Ancient homomorphy of molluscan sex chromosomes sustained by reversible sex-biased genes and sex determiner translocation. *Nat. Ecol. Evol.* **6**, 1891–1906 (2022).
17. H. P. Yazdi, H. Ellegren, Old but not (so) degenerated—Slow evolution of largely homomorphic sex chromosomes in ratites. *Mol. Biol. Evol.* **31**, 1444–1453 (2014).
18. S. Xie, J. Li, W. Chen, L. J. M. Fong, C. Huang, Y. Feng, Q. Ai, M. Zhao, J. E. Mank, H. Wu, Extreme heterochiasmy and high rates of sex-reversed recombination result in large yet homomorphic sex chromosomes in the Emei moustache toad. *Genome Res.* **35**, 1325–1336 (2025).
19. P. Jay, D. L. Jeffries, F. E. Hartmann, A. Véber, T. Giraud, Why do sex chromosomes progressively lose recombination? *Trends Genet.* **40**, 564–579 (2024).
20. D. L. Jeffries, J. F. Gerchen, M. Scharmann, J. R. Pannell, A neutral model for the loss of recombination on sex chromosomes. *Philos. Trans. R. Soc. Lond. B Biol. Sci.* **376**, 20200096 (2021).
21. T. Lenormand, D. Roze, Y recombination arrest and degeneration in the absence of sexual dimorphism. *Science* **375**, 663–666 (2022).
22. D. Charlesworth, When and how do sex-linked regions become sex chromosomes? *Evolution* **75**, 569–581 (2021).
23. Z. Wang, J. Zhang, X. Xu, C. Witt, Y. Deng, G. Chen, G. Meng, S. Feng, L. Xu, T. Szekely, G. Zhang, Q. Zhou, Phylogeny and sex chromosome evolution of Palaeognathae. *J. Genet. Genomics* **49**, 109–119 (2022).
24. G. Dixon, J. Kitano, M. Kirkpatrick, The origin of a new sex chromosome by introgression between two stickleback fishes. *Mol. Biol. Evol.* **36**, 28–38 (2019).
25. H. M. Natri, J. Merilä, T. Shikano, The evolution of sex determination associated with a chromosomal inversion. *Nat. Commun.* **10**, 145 (2019).
26. X. Yi, D. Wang, K. Reid, X. Feng, A. Löytynoja, J. Merilä, Sex chromosome turnover in hybridizing stickleback lineages. *Evol. Lett.* **8**, 360–371 (2024).

27. Z. Liu, A. L. Herbert, Y. F. Chan, M. Kučka, D. M. Kingsley, C. L. Peichel, The fourspine stickleback (*Apeltes quadracus*) has an XY sex chromosome system with polymorphic inversions on both X and Y chromosomes. *PLOS Genet.* **21**, e1011465 (2025).
28. J. M. Sardell, M. P. Josephson, A. C. Dalziel, C. L. Peichel, M. Kirkpatrick, Heterogeneous histories of recombination suppression on stickleback sex chromosomes. *Mol. Biol. Evol.* **38**, 4403–4418 (2021).
29. D. L. Jeffries, J. A. Mee, C. L. Peichel, Identification of a candidate sex determination gene in *Culaea inconstans* suggests convergent recruitment of an Amh duplicate in two lineages of stickleback. *J. Evol. Biol.* **35**, 1683–1695 (2022).
30. C. L. Peichel, S. R. McCann, J. A. Ross, A. F. S. Naftaly, J. R. Urton, J. N. Cech, J. Grimwood, J. Schmutz, R. M. Myers, D. M. Kingsley, M. A. White, Assembly of the threespine stickleback Y chromosome reveals convergent signatures of sex chromosome evolution. *Genome Biol.* **21**, 177 (2020).
31. B. Guo, B. Fang, T. Shikano, P. Momigliano, C. Wang, A. Kravchenko, J. Merilä, A phylogenomic perspective on diversity, hybridization and evolutionary affinities in the stickleback genus *Pungitius*. *Mol. Ecol.* **28**, 4046–4064 (2019).
32. Y. Wang, Y. Wang, Y. Zhao, A. Y. Kravchenko, J. Merilä, B. Guo, Phylogenomics of northeast Asian *Pungitius* sticklebacks. *Div. Distrib.* **28**, 2610–2621 (2022).
33. Y. Wang, Y. Wang, X. Cheng, Y. Ding, C. Wang, J. Merilä, B. Guo, Prevalent introgression underlies convergent evolution in the diversification of *Pungitius* sticklebacks. *Mol. Biol. Evol.* **40**, msad026 (2023).
34. F. A. Simão, R. M. Waterhouse, P. Ioannidis, E. V. Kriventseva, E. M. Zdobnov, BUSCO: Assessing genome assembly and annotation completeness with single-copy orthologs. *Bioinformatics* **31**, 3210–3212 (2015).
35. M. Kivikoski, P. Rastas, A. Löytynoja, J. Merilä, Automated improvement of stickleback reference genome assemblies with Lep-Anchor software. *Mol. Ecol. Resour.* **21**, 2166–2176 (2021).
36. Z. Liu, M. Roesti, D. Marques, M. Hiltbrunner, V. Saladin, C. L. Peichel, Chromosomal fusions facilitate adaptation to divergent environments in threespine stickleback. *Mol. Biol. Evol.* **39**, msab358 (2022).
37. J. Kitano, S. Mori, C. L. Peichel, Sexual dimorphism in the external morphology of the threespine stickleback (*Gasterosteus aculeatus*). *Copeia* **2007**, 336–349 (2007).
38. J. McKenzie, M. Keenleyside, Reproductive behavior of ninespine sticklebacks (*Pungitius pungitius* (L.)) in South Bay, Manitoulin Island, Ontario. *Can. J. Zool.* **48**, 55–61 (2011).
39. J. Yang, B. Guo, T. Shikano, X. Liu, J. Merilä, Quantitative trait locus analysis of body shape divergence in nine-spined sticklebacks based on high-density SNP-panel. *Sci. Rep.* **6**, 26632 (2016).
40. P. J. Seear, E. Rosato, W. P. Goodall-Copestake, I. Barber, The molecular evolution of spiggin nesting glue in sticklebacks. *Mol. Ecol.* **24**, 4474–4488 (2015).
41. Y. Sheng, B. Chen, L. Zhang, M. Luo, H. Cheng, R. Zhou, Identification of Dmrt genes and their up-regulation during gonad transformation in the swamp eel (*Monopterus albus*). *Mol. Biol. Rep.* **41**, 1237–1245 (2014).
42. A. Yamaguchi, K. H. Lee, H. Fujimoto, K. Kadomura, S. Yasumoto, M. Matsuyama, Expression of the DMRT gene and its roles in early gonadal development of the Japanese pufferfish *Takifugu rubripes*. *Comp. Biochem. Physiol. Part D Genomics Proteomics* **1**, 59–68 (2006).
43. K. Kashimada, T. Svingen, C.-W. Feng, E. Pelosi, S. Bagheri-Fam, V. R. Harley, D. Schlessinger, J. Bowles, P. Koopman, Antagonistic regulation of Cyp26b1 by transcription factors SOX9/SF1 and FOXL2 during gonadal development in mice. *FASEB J.* **25**, 3561–3569 (2011).
44. G. Yu, X. Liu, D. Zhang, J. Wang, G. Ouyang, Z. Chen, W. Xiao, Zebrafish Nedd8 facilitates ovarian development and the maintenance of female secondary sexual characteristics via suppression of androgen receptor activity. *Development* **147**, dev194886 (2020).
45. P. Lorès, D. Dacheux, Z.-E. Kherraf, J.-F. Nsota Mbango, C. Coutton, L. Stouvenel, C. Ialy-Radio, A. Amiri-Yekta, M. Whitfield, A. Schmitt, C. Cazin, M. Givelet, L. Ferreux, S. Fourati Ben, Mustapha, L. Halouani, O. Marrakchi, A. Daneshipour, E. El Khouri, M. Do Cruzeiro, M. Favier, F. Guillonneau, M. Chaudhry, Z. Sakheli, J.-P. Wolf, C. Patrat, G. Gacon, S. N. Savinov, S. H. Hosseini, D. R. Robinson, R. Zouari, A. Ziyyat, C. Arnoult, E. Dulioust, M. Bonhivers, P. F. Ray, A. Touré, Mutations in TTC29, encoding an evolutionarily conserved axonemal protein, result in asthenozoospermia and male infertility. *Am. J. Hum. Genet.* **105**, 1148–1167 (2019).
46. W. Tao, J. Chen, D. Tan, J. Yang, L. Sun, J. Wei, M. A. Conte, T. D. Kocher, D. Wang, Transcriptome display during tilapia sex determination and differentiation as revealed by RNA-Seq analysis. *BMC Genomics* **19**, 363 (2018).
47. K. Ożegowska, M. Dyszkiewicz-Konwińska, P. Celichowski, M. J. Nawrocki, A. Bryja, M. Jankowski, W. Kranc, M. Brązert, S. Knap, M. Jeseta, M. T. Skowroński, D. Bukowska, P. Antosik, K. P. Brüssow, A. Bręborowicz, M. Bruska, M. Nowicki, L. Pawelczyk, M. Zabel, B. Kempisty, Expression pattern of new genes regulating female sex differentiation and in vitro maturational status of oocytes in pigs. *Theriogenology* **121**, 122–133 (2018).
48. C. Yang, L. Chen, R. Huang, B. Gui, Y. Li, Y. Li, Y. Li, L. Liao, Z. Zhu, Y. Wang, Screening of genes related to sex determination and differentiation in Mandarin fish (*Siniperca chuatsi*). *Int. J. Mol. Sci.* **23**, 7692 (2022).
49. T. Wu, Y. Cheng, Z. Liu, W. Tao, S. Zheng, D. Wang, Bioinformatic analyses of zona pellucida genes in vertebrates and their expression in Nile tilapia. *Fish Physiol. Biochem.* **44**, 435–449 (2018).
50. P. Zheng, J. Dean, Oocyte-specific genes affect folliculogenesis, fertilization, and early development. *Semin. Reprod. Med.* **25**, 243–251 (2007).
51. H. Luo, Y. Li, S. Zheng, J. Zhou, X. Zou, C. Li, H. Ye, Z. Li, C. Zhou, G. Lv, S. Xiao, H. Ye, Identification of male sex-specific markers using genome re-sequencing in the Chinese longsnout catfish *Leiocassis longirostris*. *Aquaculture* **558**, 738392 (2022).
52. S. Prasertlux, K. Sittikankaew, P. Chumtong, B. Khamnamtong, S. Klinbunga, Molecular characterization and expression of the *Prostaglandin reductase 1* gene and protein during ovarian development of the giant tiger shrimp *Penaeus monodon*. *Aquaculture* **322-323**, 134–141 (2011).
53. K. L. Ayers, L. S. Lambeth, N. M. Davidson, A. H. Sinclair, A. Oshlack, C. A. Smith, Identification of candidate gonadal sex differentiation genes in the chicken embryo using RNA-seq. *BMC Genomics* **16**, 704 (2015).
54. S. Nef, O. Schaad, N. R. Stallings, C. R. Cederroth, J.-L. Pitetti, G. Schaer, S. Malki, M. Dubois-Dauphin, B. Boizet-Bonhoure, P. Descombes, K. L. Parker, J.-D. Vassalli, Gene expression during sex determination reveals a robust female genetic program at the onset of ovarian development. *Dev. Biol.* **287**, 361–377 (2005).
55. T. Kobayashi, M. Matsuda, H. Kajiura-Kobayashi, A. Suzuki, N. Saito, M. Nakamoto, N. Shibata, Y. Nagahama, Two DM domain genes, DMY and DMRT1, involved in testicular differentiation and development in the medaka. *Oryzias latipes*. *Dev. Dyn.* **231**, 518–526 (2004).
56. B. S. Chae, H. J. Yang, Sexual dimorphism in eightspine stickleback, *Pungitius sinensis*: Gasterosteidae. *Korean J. Zool.* **33**, 260–265 (1990).
57. J. E. Mank, The transcriptional architecture of phenotypic dimorphism. *Nat. Ecol. Evol.* **1**, 0006 (2017).
58. T. V. Kent, J. Uzunović, S. I. Wright, Coevolution between transposable elements and recombination. *Philos. Trans. R. Soc. Lond. B Biol. Sci.* **372**, 20160458 (2017).
59. T. Wicker, F. Sabot, A. Hua-Van, J. L. Bennetzen, P. Capy, B. Chalhoub, A. Flavell, P. Leroy, M. Morgante, O. Panaud, E. Paux, P. SanMiguel, A. H. Schulman, A unified classification system for eukaryotic transposable elements. *Nat. Rev. Genet.* **8**, 973–982 (2007).
60. Y. Jung, H. Bang, Y.-H. Kim, N.-E. Park, Y.-H. Park, C. Park, S.-R. Lee, J.-W. Lee, B.-S. Song, J.-S. Kim, B.-W. Sim, D.-W. Seol, G. Wee, S. Kim, S.-U. Kim, E. Kim, V-set and immunoglobulin domain-containing 1 (VSIG1), predominantly expressed in testicular germ cells, is dispensable for spermatogenesis and male fertility in mice. *Animals* **11**, 1037 (2021).
61. G. S. van Doorn, M. Kirkpatrick, Transitions between male and female heterogamety caused by sex-antagonistic selection. *Genetics* **186**, 629–645 (2010).
62. G. S. van Doorn, M. Kirkpatrick, Turnover of sex chromosomes induced by sexual conflict. *Nature* **449**, 909–912 (2007).
63. O. Blaser, S. Neuenschwander, N. Perrin, Sex-chromosome turnovers: The hot-potato model. *Am. Nat.* **183**, 140–146 (2014).
64. A. E. Wright, I. Darolti, N. I. Bloch, V. Oostra, B. Sandkam, S. D. Buechel, N. Kolm, F. Breden, B. Vicoso, J. E. Mank, Convergent recombination suppression suggests role of sexual selection in guppy sex chromosome formation. *Nat. Commun.* **8**, 14251 (2017).
65. S. H. Smith, K. Hsiung, A. Böhne, Evaluating the role of sexual antagonism in the evolution of sex chromosomes: New data from fish. *Curr. Opin. Genet. Dev.* **81**, 102078 (2023).
66. P. D. Price, S. M. Parkus, A. E. Wright, Recent progress in understanding the genomic architecture of sexual conflict. *Curr. Opin. Genet. Dev.* **80**, 102047 (2023).
67. S. H. Smith, K. Hsiung, A. Böhne, Evaluating the role of sexual antagonism in the evolution of sex chromosomes: New data from fish. *Curr. Opin. Genet. Dev*. **81**, 102078 (2023).
68. Y. Sun, J. Svedberg, M. Hiltunen, P. Corcoran, H. Johannesson, Large-scale suppression of recombination predates genomic rearrangements in *Neurospora tetrasperma*. *Nat. Commun.* **8**, 1140 (2017).
69. S. Adolfsson, H. Ellegren, Lack of dosage compensation accompanies the arrested stage of sex chromosome evolution in ostriches. *Mol. Biol. Evol.* **30**, 806–810 (2013).
70. N. Rodrigues, T. Studer, C. Dufresnes, N. Perrin, Sex-chromosome recombination in common frogs brings water to the fountain-of-youth. *Mol. Biol. Evol.* **35**, 942–948 (2018).
71. S. Ou, W. Su, Y. Liao, K. Chougule, J. R. A. Agda, A. J. Hellinga, C. S. B. Lugo, T. A. Elliott, D. Ware, T. Peterson, N. Jiang, C. N. Hirsch, M. B. Hufford, Benchmarking transposable element annotation methods for creation of a streamlined, comprehensive pipeline. *Genome Biol.* **20**, 275 (2019).
72. S. Álvarez-Carretero, P. Kapli, Z. Yang, Beginner's guide on the use of PAML to detect positive selection. *Mol. Biol. Evol.* **40**, msad041 (2023).
73. M. Kimura, A simple method for estimating evolutionary rates of base substitutions through comparative studies of nucleotide sequences. *J. Mol. Evol.* **16**, 111–120 (1980).
74. B. Guo, F. J. Chain, E. Bornberg-Bauer, E. H. Leder, J. Merilä, Genomic divergence between nine- and three-spined sticklebacks. *BMC Genomics* **14**, 756 (2013).
75. S. Chen, Y. Zhou, Y. Chen, J. Gu, fastp: An ultra-fast all-in-one FASTQ preprocessor. *Bioinformatics* **34**, i884–i890 (2018).

76. G. Marçais, C. Kingsford, A fast, lock-free approach for efficient parallel counting of occurrences of *k*-mers. *Bioinformatics* **27**, 764–770 (2011).
77. G. W. Vurture, F. J. Sedlazeck, M. Nattestad, C. J. Underwood, H. Fang, J. Gurtowski, M. C. Schatz, GenomeScope: Fast reference-free genome profiling from short reads. *Bioinformatics* **33**, 2202–2204 (2017).
78. J. Hu, Z. Wang, Z. Sun, B. Hu, A. O. Ayoola, F. Liang, J. Li, J. R. Sandoval, D. N. Cooper, K. Ye, J. Ruan, C.-L. Xiao, D. Wang, D.-D. Wu, S. Wang, NextDenovo: An efficient error correction and accurate assembly tool for noisy long reads. *Genome Biol.* **25**, 107 (2024).
79. H. Cheng, G. T. Concepcion, X. Feng, H. Zhang, H. Li, Haplotype-resolved de novo assembly using phased assembly graphs with hifiasm. *Nat. Methods* **18**, 170–175 (2021).
80. R. Vaser, I. Sovic, N. Nagarajan, M. Sikic, Fast and accurate de novo genome assembly from long uncorrected reads. *Genome Res.* **27**, 737–746 (2017).
81. B. J. Walker, T. Abeel, T. Shea, M. Priest, A. Abouelliel, S. Sakthikumar, C. A. Cuomo, Q. Zeng, J. Wortman, S. K. Young, A. M. Earl, Pilon: An Integrated tool for comprehensive microbial variant detection and genome assembly improvement. *PLOS ONE* **9**, e112963 (2014).
82. O. Dudchenko, S. S. Batra, A. D. Omer, S. K. Nyquist, M. Hoeger, N. C. Durand, M. S. Shamim, I. Machol, E. S. Lander, A. P. Aiden, E. L. Aiden, De novo assembly of the Aedes aegypti genome using Hi-C yields chromosome-length scaffolds. *Science* **356**, 92–95 (2017).
83. N. C. Durand, M. S. Shamim, I. Machol, S. S. P. Rao, M. H. Huntley, E. S. Lander, E. L. Aiden, Juicer provides a one-click system for analyzing loop-resolution Hi-C experiments. *Cell Syst.* **3**, 95–98 (2016).
84. N. C. Durand, J. T. Robinson, M. S. Shamim, I. Machol, J. P. Mesirov, E. S. Lander, E. L. Aiden, Juicebox provides a visualization system for Hi-C contact maps with unlimited zoom. *Cell Syst.* **3**, 99–101 (2016).
85. D. Kim, J. M. Paggi, C. Park, C. Bennett, S. L. Salzberg, Graph-based genome alignment and genotyping with HISAT2 and HISAT-genotype. *Nat. Biotechnol.* **37**, 907–915 (2019).
86. M. Pertea, G. M. Pertea, C. M. Antonescu, T.-C. Chang, J. T. Mendell, S. L. Salzberg, StringTie enables improved reconstruction of a transcriptome from RNA-seq reads. *Nat. Biotechnol.* **33**, 290–295 (2015).
87. M. Stanke, O. Keller, I. Gunduz, A. Hayes, S. Waack, B. Morgenstern, AUGUSTUS: Ab initio prediction of alternative transcripts. *Nucleic Acids Res.* **34**, W435–W439 (2006).
88. J. Keilwagen, F. Hartung, J. Grau, "GeMoMa: Homology-based gene prediction utilizing intron position conservation and RNA-seq data," in *Gene Prediction: Methods and Protocols*, M. Kollmar, Ed. (Springer, 2019), pp. 161–177.
89. T. Paysan-Lafosse, M. Blum, S. Chuguransky, T. Grego, B. L. Pinto, G. A. Salazar, M. L. Bileschi, P. Bork, A. Bridge, L. Colwell, J. Gough, D. H. Haft, I. Letunić, A. Marchler-Bauer, H. Mi, D. A. Natale, C. A. Orengo, A. P. Pandurangan, C. Rivoire, C. J. A. Sigrist, I. Sillitoe, N. Thanki, P. D. Thomas, S. C. E. Tosatto, C. H. Wu, A. Bateman, InterPro in 2022. *Nucleic Acids Res.* **51**, D418–D427 (2023).
90. D. M. Emms, S. Kelly, OrthoFinder: Phylogenetic orthology inference for comparative genomics. *Genome Biol.* **20**, 238 (2019).
91. Q. Li, D. Lindtke, C. Rodríguez-Ramírez, R. Kakioka, H. Takahashi, A. Toyoda, J. Kitano, R. L. Ehrlich, J. Chang Mell, S. Yeaman, Local adaptation and the evolution of genome architecture in threespine stickleback. *Genome Biol. Evol.* **14**, evac075 (2022).
92. R. C. Edgar, MUSCLE: Multiple sequence alignment with high accuracy and high throughput. *Nucleic Acids Res.* **32**, 1792–1797 (2004).
93. G. Talavera, J. Castresana, Improvement of phylogenies after removing divergent and ambiguously aligned blocks from protein sequence alignments. *Syst. Biol.* **56**, 564–577 (2007).
94. B. Q. Minh, H. A. Schmidt, O. Chernomor, D. Schrempf, M. D. Woodhams, A. von Haeseler, R. Lanfear, IQ-TREE 2: New models and efficient methods for phylogenetic inference in the genomic era. *Mol. Biol. Evol.* **37**, 1530–1534 (2020).
95. Z. Yang, PAML 4: Phylogenetic analysis by maximum likelihood. *Mol. Biol. Evol.* **24**, 1586–1591 (2007).
96. S. Kumar, G. Stecher, M. Suleski, S. B. Hedges, TimeTree: A resource for timelines, timetrees, and divergence times. *Mol. Biol. Evol.* **34**, 1812–1819 (2017).
97. S. E. Rawlinson, M. A. Bell, A stickleback fish (*Pungitius*) from the Neogene Sterling Formation, Kenai Peninsula, Alaska. *J. Paleontol.* **56**, 583–588 (1982).
98. H.-G. Bae, H. Y. Suk, Population genetic structure and colonization history of short ninespine sticklebacks (*Pungitius kaibarae*). *Ecol. Evol.* **5**, 3075–3089 (2015).
99. H. Tang, V. Krishnakumar, X. Zeng, Z. Xu, A. Taranto, J. S. Lomas, Y. Zhang, Y. Huang, Y. Wang, W. C. Yim, J. Zhang, X. Zhang, JCVI: A versatile toolkit for comparative genomics analysis. *iMeta* **3**, e211 (2024).
100. M. Krzywinski, J. Schein, İ. Birol, J. Connors, R. Gascoyne, D. Horsman, S. J. Jones, M. A. Marra, Circos: An information aesthetic for comparative genomics. *Genome Res.* **19**, 1639–1645 (2009).
101. R. S. Harris, "Improved pairwise alignment of genomic DNA," thesis, Pennsylvania State University, University Park, PA (2007).
102. H. Li, Minimap2: Pairwise alignment for nucleotide sequences. *Bioinformatics* **34**, 3094–3100 (2018).
103. J. T. Robinson, H. Thorvaldsdóttir, W. Winckler, M. Guttman, E. S. Lander, G. Getz, J. P. Mesirov, Integrative genomics viewer. *Nat. Biotechnol.* **29**, 24–26 (2011).
104. H. Li, R. Durbin, Fast and accurate short read alignment with Burrows–Wheeler transform. *Bioinformatics* **25**, 1754–1760 (2009).
105. P. Danecek, J. K. Bonfield, J. Liddle, J. Marshall, V. Ohan, M. O. Pollard, A. Whitwham, T. Keane, S. A. McCarthy, R. M. Davies, H. Li, Twelve years of SAMtools and BCFtools. *GigaScience* **10**, giab008 (2021).
106. J. J. Smith, N. Timoshevskaya, C. Ye, C. Holt, M. C. Keinath, H. J. Parker, M. E. Cook, J. E. Hess, S. R. Narum, F. Lamanna, H. Kaessmann, V. A. Timoshevskiy, C. K. M. Waterbury, C. Saraceno, L. M. Wiedemann, S. M. C. Robb, C. Baker, E. E. Eichler, D. Hockman, T. Sauka-Spengler, M. Yandell, R. Krumlauf, G. Elgar, C. T. Amemiya, The sea lamprey germline genome provides insights into programmed genome rearrangement and vertebrate evolution. *Nat. Genet.* **50**, 270–277 (2018).
107. P. Danecek, A. Auton, G. Abecasis, C. A. Albers, E. Banks, M. A. DePristo, R. E. Handsaker, G. Lunter, G. T. Marth, S. T. Sherry, G. McVean, R. Durbin, The variant call format and VCFtools. *Bioinformatics* **27**, 2156–2158 (2011).
108. S. Purcell, B. Neale, K. Todd-Brown, L. Thomas, M. A. R. Ferreira, D. Bender, J. Maller, P. Sklar, P. I. W. de Bakker, M. J. Daly, P. C. Sham, PLINK: A tool set for whole-genome association and population-based linkage analyses. *Am. J. Hum. Genet.* **81**, 559–575 (2007).
109. S. R. Browning, B. L. Browning, Rapid and accurate haplotype phasing and missing-data inference for whole-genome association studies by use of localized haplotype clustering. *Am. J. Hum.* **81**, 1084–1097 (2007).
110. D. E. Cook, E. C. Andersen, VCF-kit: Assorted utilities for the variant call format. *Bioinformatics* **33**, 1581–1582 (2017).
111. W. Shen, S. Le, Y. Li, F. Hu, SeqKit: A cross-platform and ultrafast toolkit for FASTA/Q file manipulation. *PLOS ONE* **11**, e0163962 (2016).
112. M. N. Price, P. S. Dehal, A. P. Arkin, FastTree 2—Approximately maximum-likelihood trees for large alignments. *PLOS ONE* **5**, e9490 (2010).
113. C.-S. Chin, P. Peluso, F. J. Sedlazeck, M. Nattestad, G. T. Concepcion, A. Clum, C. Dunn, R. O'Malley, R. Figueroa-Balderas, A. Morales-Cruz, G. R. Cramer, M. Delledonne, C. Luo, J. R. Ecker, D. Cantu, D. R. Rank, M. C. Schatz, Phased diploid genome assembly with single molecule real-time sequencing. *Nat. Methods* **13**, 1050–1054 (2016).
114. M. Alonge, L. Lebeigle, M. Kirsche, K. Jenike, S. Ou, S. Aganezov, X. Wang, Z. B. Lippman, M. C. Schatz, S. Soyk, Automated assembly scaffolding using RagTag elevates a new tomato system for high-throughput genome editing. *Genome Biol.* **23**, 258 (2022).
115. S. Kurtz, A. Phillippy, A. L. Delcher, M. Smoot, M. Shumway, C. Antonescu, S. L. Salzberg, Versatile and open software for comparing large genomes. *Genome Biol.* **5**, R12 (2004).
116. H. Wickham, *Ggplot2: Elegant Graphics for Data Analysis* (Springer International Publishing, 2016).
117. M. A. White, J. Kitano, C. L. Peichel, Purifying selection maintains dosage-sensitive genes during degeneration of the threespine stickleback Y chromosome. *Mol. Biol. Evol.* **32**, 1981–1995 (2015).
118. Y. Wang, Y. Zhao, Y. Wang, Z. Li, B. Guo, J. Merilä, Population transcriptomics reveals weak parallel genetic basis in repeated marine and freshwater divergence in nine-spined sticklebacks. *Mol. Ecol.* **29**, 1642–1656 (2020).
119. M. I. Love, W. Huber, S. Anders, Moderated estimation of fold change and dispersion for RNA-seq data with DESeq2. *Genome Biol.* **15**, 550 (2014).
120. T. Wu, E. Hu, S. Xu, M. Chen, P. Guo, Z. Dai, T. Feng, L. Zhou, W. Tang, L. Zhan, X. Fu, S. Liu, X. Bo, G. Yu, clusterProfiler 4.0: A universal enrichment tool for interpreting omics data. *Innovation* **2**, 100141 (2021).
121. J. Teng, Y. Zhao, H. J. Chen, L. Y. Xue, X. S. Ji, Global expression response of genes in sex-undifferentiated Nile tilapia gonads after exposure to trace letrozole. *Ecotoxicol. Environ. Saf.* **217**, 112255 (2021).
122. Z. Li, J. Jia, J. Gou, X. Zhao, T. Yi, MicroRNA-451 plays a role in murine embryo implantation through targeting Ankrd46, as implicated by a microarray-based analysis. *Fertil. Steril.* **103**, 834–844.e4 (2015).
123. H. Zhang, C. Situ, X. Guo, Recent progress of proteomic analysis on spermatogenesis. *Biol. Reprod.* **107**, 109–117 (2022).
124. M. C. Hale, P. Xu, J. Scardina, P. A. Wheeler, G. H. Thorgaard, K. M. Nichols, Differential gene expression in male and female rainbow trout embryos prior to the onset of gross morphological differentiation of the gonads. *BMC Genomics* **12**, 404 (2011).
125. M.-Y. Hu, J. Yu, J.-Q. Lin, S.-G. Fang, Sex-biased miRNAs in the gonads of adult Chinese alligator (*Alligator sinensis*) and their potential roles in sex maintenance. *Front. Genet.* **13**, 843884 (2022).
126. R. Wang, X. Liu, L. Li, M. Yang, J. Yong, F. Zhai, L. Wen, L. Yan, J. Qiao, F. Tang, Dissecting human gonadal cell lineage specification and sex determination using a single-cell RNA-seq approach. *Genom. Proteom. Bioinform.* **20**, 223–245 (2022).
127. Y.-H. Yang, R. Wang, M. Li, H.-Z. Yang, G.-H. Huang, K.-Y. Ma, G.-F. Qiu, Y. Lin, Comparative transcriptomes analysis of the ovary reveals potential ovarian development-related genes and pathways in *Macrobrachium rosenbergii*. *Invertebr. Reprod. Dev.* **67**, 13–25 (2023).

128. S. Kassel, A. J. Hanson, H. Benchabane, K. Saito-Diaz, C. R. Cabel, L. Goldsmith, M. Taha, A. Kanuganti, V. H. Ng, G. Xu, F. Ye, J. Picker, F. Port, M. Boutros, V. L. Weiss, D. J. Robbins, C. A. Thorne, Y. Ahmed, E. Lee, USP47 deubiquitylates Groucho/TLE to promote Wnt–β-catenin signaling. *Sci. Signal.* **16**, eabn8372 (2023).
129. M. Ding, X.-Y. Li, Z.-X. Zhu, J.-H. Chen, M. Lu, Q. Shi, Y. Wang, Z. Li, X. Zhao, T. Wang, W.-X. Du, C. Miao, T.-Z. Yao, M.-T. Wang, X.-J. Zhang, Z.-W. Wang, L. Zhou, J.-F. Gui, Genomic anatomy of male-specific microchromosomes in a gynogenetic fish. *PLOS Genet.* **17**, e1009760 (2021).
130. J. Brennan, J. Karl, B. Capel, Divergent vascular mechanisms downstream of *Sry* establish the arterial system in the XY gonad. *Dev. Biol.* **244**, 418–428 (2002).
131. R. Llera-Herrera, A. García-Gasca, C. Abreu-Goodger, A. Huvet, A. M. Ibarra, Identification of male gametogenesis expressed genes from the scallop *Nodipecten subnodosus* by suppressive subtraction hybridization and pyrosequencing. *PLOS ONE* **8**, e73176 (2013).
132. H. Xia, C. Zhong, X. Wu, J. Chen, B. Tao, X. Xia, M. Shi, Z. Zhu, V. L. Trudeau, W. Hu, Mettl3 mutation disrupts gamete maturation and reduces fertility in zebrafish. *Genetics* **208**, 729–743 (2018).
133. G. Varuzhanyan, M. S. Ladinsky, S. Yamashita, M. Abe, K. Sakimura, T. Kanki, D. C. Chan, Fis1 ablation in the male germline disrupts mitochondrial morphology and mitophagy, and arrests spermatid maturation. *Development* **148**, dev199686 (2021).
134. J. W. Bergs, N. Neuendorff, G. van der Heijden, E. Wassenaar, P. Rexin, H.-P. Elsässer, R. Moll, W. M. Baarends, A. Brehm, Differential expression and sex chromosome association of CHD3/4 and CHD5 during spermatogenesis. *PLOS ONE* **9**, e98203 (2014).
135. X. Xu, J. K. Coats, C. F. Yang, A. Wang, O. M. Ahmed, M. Alvarado, T. Izumi, N. M. Shah, Modular genetic control of sexually dimorphic behaviors. *Cell* **148**, 596–607 (2012).
136. J. Jones, P. M. Macdonald, Neurl4 contributes to germ cell formation and integrity in *Drosophila*. *Biol. Open* **4**, 937–946 (2015).
137. M. Wang, L. Li, H. Lin, Z. Zhou, B. Liu, J. Zhong, F. Pu, Y. Shi, T. Zhou, P. Xu, Genome-wide association study identifies genomic loci of sex determination, gonadal weight and gonadosomatic index traits in *Takifugu bimaculatus*. *Aquaculture* **546**, 737389 (2022).
138. M. Paz, A. Mikhailov, M. Torrado, Sexual differentiation of the somatic gonad tissue in marine bivalve mollusks: Esterase- and fibronectin-like recognition signals. *Int. J. Dev. Biol.* **45**, S119–S120 (2001).
139. S. S. Tanaka, A. Nakane, Y. L. Yamaguchi, T. Terabayashi, T. Abe, K. Nakao, M. Asashima, K. A. Steiner, P. P. L. Tam, R. Nishinakamura, Dullard/Ctdnep1 modulates WNT signalling activity for the formation of primordial germ cells in the mouse embryo. *PLOS ONE* **8**, e57428 (2013).
140. R. Zachow, M. Uzumcu, The hepatocyte growth factor system as a regulator of female and male gonadal function. *J. Endocrinol.* **195**, 359–371 (2007).
141. K. Yonehara, M. Suzuki, K. Yamanouchi, M. Nishihara, Expression analyses of sex steroid-regulated genes in neonatal rat hypothalamus. *J. Reprod. Dev.* **49**, 547–552 (2003).
142. J. B. Fitzgerald, J. George, L. K. Christenson, Non-coding RNA in ovarian development and disease. *Adv. Exp. Med. Biol.* **886**, 79–93 (2016).
143. S. Romano, O. H. Kaufman, F. L. Marlow, Loss of dmrt1 restores zebrafish female fates in the absence of *cyp19a1a* but not *rbpms2a/b*. *Development* **147**, dev190942 (2020).
144. S. W. Miller, D. C. Hayward, T. A. Bunch, D. J. Miller, E. E. Ball, V. J. Bardwell, D. Zarkower, D. L. Brower, A DM domain protein from a coral, *Acropora millepora*, homologous to proteins important for sex determination. *Evol. Dev.* **5**, 251–258 (2003).
145. E. Zaharieva, I. U. Haussmann, U. Bräuer, M. Soller, Concentration and localization of coexpressed ELAV/Hu proteins control specificity of mRNA processing. *Mol. Cell. Biol.* **35**, 3104–3115 (2015).


**Acknowledgments:** We thank H. Liu, C. Niu, and D. Qi for help in fish sampling, and members of the Guo laboratory for discussion and comments on the manuscript. **Funding:** This work was funded by the National Natural Science Foundation of China (32161160321, 32022009, and 31672273 to B.G.), the NSFC/RGC Joint Research Scheme sponsored by the Research Grants Council of the Hong Kong Special Administrative Region, China, the National Natural Science Foundation of China (N_HKU763/21 to J.M.), and the Academy of Finland (129662, 134728, and 218343 to J.M). **Author contributions:** Conceptualization: B.G., Yu Wang, and J.M. Methodology: B.G., X.C., X.L., and C.W. Software: B.G., X.C., and M.Z. Validation: B.G., X.C., and J.M. Formal analysis: B.G., X.C., M.Z., Yingnan Wang, and H.Z. Investigation: B.G., X.C., Yu Wang, Yingnan Wang, X.L., and C.W. Resources: B.G., X.C., Yingnan Wang, X.L., C.W., and J.M. Data curation: B.G., X.C., and C.W. Writing—original draft: B.G., X.C., and Yu Wang. Writing—review and editing: B.G., X.C., Yu Wang, X.L., H.Z, C.W., and J.M. Visualization: B.G., X.C., Yu Wang, and X.L. Supervision: B.G. Project administration: B.G. Funding acquisition: B.G. and J.M. **Competing interests:** The authors declare that they have no competing interests. **Data, code, and materials availability:** All data and code needed to evaluate and reproduce the results in the paper are present in the paper and/or the Supplementary Materials. All sequencing data and genome assembly data generated in this study were deposited in the National Genomics Data Center, China National Center for Bioinformation/Beijing Institute of Genomics, Chinese Academy of Sciences (https://www.cncb.ac.cn/?lang=en) under accession number PRJCA035368. These data will be publicly available upon publication. The custom scripts and associated configuration files for genome assembly and the analysis of sex chromosome generated for this study are publicly available in Zenodo (DOI: 10.5281/zenodo.19030063). All other bioinformatics analyses were performed using publicly available software. The software names, versions, and key parameters are described in Materials and Methods, with appropriate citations provided to ensure reproducibility. This study did not generate new unique materials. Commercial reagents and kits used in this study are specified in Materials and Methods and are available from their respective manufacturers.

Submitted 1 August 2025
Accepted 23 April 2026
Published 5 June 2026
10.1126/sciadv.aeb1484